DEPTH INTEGRATED EQUATIONS APPLIED TO LONGITUDINAL DISCONTINUITIES ON THE CHANNEL BED

A THESIS SUBMITTED TO
THE GRADUATE SCHOOL OF NATURAL AND APPLIED SCIENCES
OF
MIDDLE EAST TECHNICAL UNIVERSITY

BY

MARAL RAZMAND

IN PARTIAL FULFILLMENT OF THE REQUIREMENTS
FOR
THE DEGREE OF MASTER OF SCIENCE
IN
CIVIL ENGINEERING

SEPTEMBER 2015

Approval of the thesis:

DEPTH INTEGRATED EQUATIONS APPLIED TO LONGITUDINAL DISCONTINUITIES ON THE CHANNEL BED

submitted by **MARAL RAZMAND** in partial fulfillment of the requirements for the degree of **Master of Science in Civil Engineering Department, Middle East Technical University** by,

Prof. Dr. Gülbin Dural Ünver
Dean, Graduate School of **Natural and Applied Sciences**

_____

Prof. Dr. Ahmet Cevdet Yalçıner
Head of Department, **Civil Engineering**

_____

Prof. Dr. İsmail Aydın
Supervisor, **Civil Engineering Department, METU** _

Examining Committee Members:

Prof. Dr. Mustafa Göğüş
Civil Engineering Department, METU

_____

Prof. Dr. İsmail Aydın
Civil Engineering Department, METU

_____

Assoc. Prof. Dr. Mete Köken
Civil Engineering Department, METU

_____

Assist. Prof. Dr Talia Ekin Tokyay Sinha
Civil Engineering Department, METU

_____

Assist. Prof. Dr. Nuray Öktem
Mathematics Department, ÇOMU

_____

Date: 10.09.201

I hereby declare that all information in this document has been obtained and presented in accordance with academic rules and ethical conduct. I also declare that, as required by these rules and conduct, I have fully cited and referenced all material and results that are not original to this work.

Name, Last name: Maral, Razmand

Signature :

ABSTRACT

DEPTH INTEGRATED EQUATIONS APPLIED TO LONGITUDINAL DISCONTINUITIES ON THE CHANNEL BED

Maral Razmand

M.S., Department of Civil Engineering
Supervisor: Prof. Dr. İsmail Aydın

September 2015, 54 pages

Depth integrated equations can be solved over large domains to provide flood inundation maps. In urban and rural areas however, there may be numerous natural or artificial bottom boundary discontinuities in the form of rapid variations in the bed elevation. Such discontinuities cause abrupt changes in the source terms of the governing equations and can significantly affect stability and accuracy of the numerical solution. A 1D code is developed for shallow water equations using HLL approximate Riemann solver. It is applied to a dam-break case until the steady state is reached between two end boundaries and volume conserving boundary conditions has been searched. Channel beds with step-like discontinuities were also studied. It is found that bed slopes greater than 1 can cause spurious water surface oscillations in the numerical solution.

Keywords: Shallow Water Equations, Depth-Averaged Equations, Riemann Solver, Flood Waves

ÖZ

DERİNLIK İNTEGRALLİ DENKLEMLERİN KANAL TABANININDA BOYUNA SÜREKSİZLİKLERE UYGULANMASI

Maral Razmand

Yüksek Lisans, İnşaat Mühendisliği Bölümü
Tez Yöneticisi: Prof. Dr. İsmail Aydın

Eylül 2015, 54 sayfa

Derinlik integralli denklemler taşkın haritaları hazırlamak amacıyla büyük alanlar üzerinde çözülebilir. Bununla beraber, kırsal ve kentsel alanlarda yatak seviyesinde ani değişiklikler oluşturacak şekilde çok sayıda doğal veya yapay düzensizlikler olabilir. Bu tür süreksizlikler akım denklemlerinin kaynak terimlerinde hızlı değişimlere neden olur ve sayısal çözümün stabilitesini ve hassasiyetini belirgin şekilde etkileyebilir. HLL Yaklaşık Riemann Çözücüsü kullanılarak sığ su denklemleri için bir 1B kod geliştirilmiştir. Bu kod, iki uç sınır arasında kararlı duruma ulaşılıncaya kadar baraj yıkılma durumuna uygulanmış ve hacim koruyan sınır koşulları araştırılmıştır. Bunun yanı sıra, basamak benzeri süreksizlikler barındıran kanal tabanları da çalışılmıştır. 1'den büyük olan yatak eğimlerinin, sayısal çözümde gerçek olmayan su yüzeyi salınımlarına neden olabileceği saptanmıştır.

Anahtar Kelimeler: Sığ Su Denklemleri, Derinlik Entegreli Denklemler, Riemann Çözücü, Taşkın Dalgası

AKNOWLEDGEMENTS

This is the best opportunity to express my sincere gratitude to all the people who have supported me through this journey. First and foremost, I am beyond thankful to my incredible Supervisor, *Prof. Dr. İsmail Aydın* for his endeavoring guidance, valuable criticism and friendly advices during my whole graduate studies. I am truly grateful to him for sharing this knowledge and enlightening views with me. I am so honored to have this opportunity to work with him. He encouraged me to move on when I was about to give up and I could not have finished this study without his kindness.

I also would like to thank *Asst. Prof. Dr. Nuray Öktem* for brightening my darkest days and always finding a way to give hope and solving problems with her kindness and enlightening knowledge. I was so lucky to have been able to get the chance of working with her and learn from her.

I have to thank my parents for their endless love and support. I grew up cocooned in your love, comforted by your hugs and motivated by your lives. I would not be at this point of my life without you. Nobody except my parents cared so much to overlook who I was and continue believing in what I can be. To them I dedicate this thesis.

Last but not least, I would like to thank my dear partner, Amir Shaygan. I want to thank him for his endless patience and love. For always being there to help and motivate me to do my best like no one else. Thank you for believing in me even when I could not believe in myself and picking me up after of thousands times of falling down.

TABLE OF CONTENTS

ABSTRACT…….....……...v

ÖZ…….….……vi

AKNOWLEDGEMENTS…….……..….vii

TABLE OF CONTENTS…….…....…...viii

LIST OF FIGURES……...…….…….…..….x

LIST OF TABLES……..……...…….....xi

LIST OF SYMBOLS & ABBREVIATIONS……...……..xii

CHAPTERS

1. INTRODUCTION……..1

1.1 General Description of the Problem 1

1.2 Objectives of the Study 2

2. SHALLOW WATER EQUATIONS AND METHODS OF NUMERICAL SOLUTION……..5

2.1 Depth Averaged Shallow Water Equations 5

2.2 Numerical Schemes for 1D Depth Averaged Shallow Water Equations 9

2.2.1 Finite Volume Methods 9

2.2.2 Approximate Riemann Solvers 12

2.2.3 HLL Approach 17

2.2.4 MUSCL – Hancock Approach (Variable Extrapolation Approach).... 19

2.2.5 High-Resolution Schemes 21

3. NUMERICAL METHOD ADOPTED TO PRESENT PROBLEM…..25

3.1 Discretization of the 1D SWE Equations using HLL Numerical Scheme .. 25

3.2 Initial and Boundary Conditions 32

3.3 Stability Criteria 33

4. NUMERICAL SOLUTIONS FOR THE TEST CASES…….35

4.1 1D Dam Break Problem with Analytical Solutions 35

4.2 1D Dam Break Problem in a Closed Domain with Various Bed Slopes.....38

4.2.1 Effect of Mesh Size in the Solution 39

4.2.2 Effect of Bed Slope on the Solution.....41

4.3 1D Dam Break Problem over a Step in a Closed Domain 45

5. CONCLUSIONS AND RECOMMENDATIONS…….51

REFERENCES……53

LIST OF FIGURES

FIGURES

Figure 2-1 Free surface flow sketch..... 6
Figure 2-2 FVM solution sketch..... 12
Figure 2-3 The solution of Riemann problem..... 14
Figure 2-4 A geometrical sketch of dam break problem 15
Figure 2-5 Godunov's upwind method for 1D flow: (a) Control volume in x-t space, (b) Integral averages giving piecewise constant data,(c) Structure of the solution of Riemann problem at interfaces (Toro, 2001)..... 16
Figure 2-6 Two-wave Riemann solution structure for HLL method (Toro, 2001) .. 17
Figure 2-7 Three-wave Riemann solution structure for HLLC method (Toro, 2001) 18
Figure 2-8 Piecewise linear MUSCL reconstruction of data in a single cell, i (Toro, 2009) 20
Figure 2-9 MUSCL-Hancock method representation (Zoppou & Roberts, 2003) ... 21
Figure 2-10 Explanation of total variation concept 22
Figure 2-11 Limiter function comparison (Versteeg & Malalasekera, 2007) 23
Figure 4-1 Comparison between numerical and analytical solution for 1D dam break test case at T=50sec, mesh size,Δx=2.00 m , H^L=10.00 m and H^R=0.10 m (supercritical flow), results obtained via HLL method. 37
Figure 4-2 Comparison between numerical and analytical solution for 1D Dam Break test case at T=50sec, mesh size,Δx=2.00 m , H^L=10.00 m and H^R=5.00 m (subcritical flow), results obtained via HLL method. 38
Figure 4-3 Dam break with various slope grid system 39
Figure 4-4 Mesh size comparison, S_0=0.4, Δx=1.0 m 40
Figure 4-5 Mesh size comparison, S_0=0.4, Δx=5.0 m 40
Figure 4-6 Mesh size comparison, S0=0.4, Δx=10.0 m..... 41
Figure 4-7 Instantaneous water surface profiles of test case simulation to investigate the effect of bed slope on the solution, S_0=1.0 , WSL=1050 (m), WSR=1040 (m), Δx=1.0 m, (a) T=0 s (initial condition), (b) T=1 s 42
Figure 4-8 Dam break problem over a step on the bed..... 46
Figure 4-9 Bottom slope grid generation according to edge angle 47
Figure 4-10 Wave formation around the geometry discontinuity at T=7000 sec 48
Figure 4-11 Relation between ratio of wave amplitude near discontinuity to step height and step edge angle 49

LIST OF TABLES

TABLES

Table 2-1 Slope limiter functions (Versteeg & Malalasekera, 2007) 22
Table 4-1 Analytical solution for dam break problem in a wide frictionless open channel (Zoppou & Roberts, 2003)..... 36
Table 4-2 General information of test case 48

LIST OF SYMBOLS & ABBREVIATIONS

α	block face angle
A	wave amplitude
b	bed elevation
c	celerity
F	total flux vector in x direction
F'	Jacobian matrix of F
ψ	slope limiter function
G	total flux vector in y direction
g	gravitational acceleration
h	flow depth
H_s	step height
H_R	water level difference
H_w	water level on the step
L	length
λ	wave speed
n	Manning's coefficient
q	unit discharge
r	ratio of upwind difference to local difference
ρ	fluid density
S	source vector
S_0	bottom slope in x and y directions
S_f	friction slope in x and y directions
$\tau_{i,j}$	combination of viscous and turbulent stresses
U	vector of conserved variables
u	velocity component in x direction
v	velocity component in y direction
w	velocity component in z direction

CHAPTER 1

INTRODUCTION

1.1 General Description of the Problem

One of the most popular areas of interest for mathematicians and scientists is to model and simulate the behavior of flow over an arbitrary surface under specific circumstances. Over the years, by improvements in computing technology, such models have been progressed significantly. As an example, tsunamis, wind waves, ocean tide, flood, dam breaks and open channel flows around obstacles are the subjects of this sort of studies. Despite the fact that the above mentioned phenomena happen regularly in our lives, the governing equations for those events are mathematically complicated to be solved directly. Correspondingly, utilization of approximate solutions are more common and practical. A typical example for this approach is the usage of depth integrated system of nonlinear partial differential equations namely, Shallow Water Equations (SWE).

All of these environmental events follow the basic physical conservation laws such as mass, momentum and energy conservation. Hydraulic engineering is one of the fields of science which deals with water flow in either open or closed systems.

The SWE can be obtained by applying the two basic conservation laws namely, mass and momentum conservation on an appropriately chosen control volume of the problem domain. The main assumption in this derivation is the nonexistent variation of flow velocity in vertical direction which leads to the hydrostatic pressure distribution being accepted. Since the variations over the vertical is eliminated, numerical solution is simplified significantly. Pressure solution is not required. Despite the fact that the shallow water equations are simplified by eliminating the third dimension, their solution contain main physical characteristics of the flow and can give very useful information about 2D horizontal plane for many engineering applications. The water surface waves in open channel flows, for example, can be represented precisely.

One of the most important features of shallow water equations is their ability to deal with discontinuous solutions. Adopting proper shock capturing numerical methods would aid the numerical approach to solve the equations in the case of shock waves and discontinuities both in solution or flow domain. It must be noted that the depth of flow should be at least 5 to 6 times smaller than the lateral extent of the flow to justify the shallowness assumption.

SWE can describe 2D flows over horizontal domains without any violation of the assumptions in the derivation. However, when SWE applied to flow domains with large bottom slope, with curvature or flow domains with 3D obstructions, the solutions will be only approximate since hydrostatic pressure distribution assumption, in such cases, is violated. The source terms due to bed slope can be large and dominant in the governing equations which may cause unrealistic solutions for the water depth and horizontal velocity components.

1.2 Objectives of the Study

In most of the studies available in literature, homogeneous form of SWE has been studied and reported. The main goal in this study is to investigate solutions of SWE over domains with discontinuities in bed elevations. Although the bed slope is presented as a source term it can be treated in different forms in the numerical solution. In this particular study, the effect of bottom slope, discontinuity in geometry as a step on the bed level, and variable slopes will be investigated. Idealized 1D dam break analysis will be conducted in a limited domain from initial hydrostatic case to final hydrostatic case after sudden dam failure. Appropriate boundary conditions will also be investigated.

In the first chapter, general information and the main idea behind this study has been given. In the second chapter, firstly the governing equations will be introduced, then their characteristics and the main assumptions will be discussed. After basic concepts, available numerical solution schemes are introduced.

In Chapter 3, the numerical solution method adopted to the present problem, discretization of the equations with initial and boundary condition, is described in a

more detailed manner. At the last section of this chapter stability criteria is presented.

Chapter 4 is reserved to present results of all test cases that have been studied where available analytical and numerical solutions are compared. Finally, reached conclusions in this study and recommendations for future works are presented in Chapter 5.

CHAPTER 2

SHALLOW WATER EQUATIONS AND METHODS OF NUMERICAL SOLUTION

2.1 Depth Averaged Shallow Water Equations

In general fluid flow is governed by Navier-Stokes equations. Basically the Reynolds Averaged Navier-Stokes (RANS) equations (Versteeg & Malalasekera, 2007) for 3D incompressible turbulent flows can be written as

$$\frac{\partial \overline{u}}{\partial x}+\frac{\partial \overline{v}}{\partial y}+\frac{\partial \overline{w}}{\partial z}=0 \tag{2.1}$$

$$\frac{\partial \overline{u}}{\partial t}+\overline{u}\frac{\partial \overline{u}}{\partial x}+\overline{v}\frac{\partial \overline{u}}{\partial y}+\overline{w}\frac{\partial \overline{u}}{\partial z}=-\frac{1}{\rho}\frac{\partial \overline{p}}{\partial x}+\frac{1}{\rho}(\frac{\partial \tau_{xx}}{\partial x}+\frac{\partial \tau_{yx}}{\partial y}+\frac{\partial \tau_{zx}}{\partial z}) \tag{2.2}$$

$$\frac{\partial \overline{v}}{\partial t}+\overline{u}\frac{\partial \overline{v}}{\partial x}+\overline{v}\frac{\partial \overline{v}}{\partial y}+\overline{w}\frac{\partial \overline{v}}{\partial z}=-\frac{1}{\rho}\frac{\partial \overline{p}}{\partial y}+\frac{1}{\rho}(\frac{\partial \tau_{xy}}{\partial x}+\frac{\partial \tau_{yy}}{\partial y}+\frac{\partial \tau_{zy}}{\partial z}) \tag{2.3}$$

$$\frac{\partial \overline{w}}{\partial t}+\overline{u}\frac{\partial \overline{w}}{\partial x}+\overline{v}\frac{\partial \overline{w}}{\partial y}+\overline{w}\frac{\partial \overline{w}}{\partial z}=-g-\frac{1}{\rho}\frac{\partial \overline{p}}{\partial z}+\frac{1}{\rho}(\frac{\partial \tau_{xz}}{\partial x}+\frac{\partial \tau_{yz}}{\partial y}+\frac{\partial \tau_{zz}}{\partial z}) \tag{2.4}$$

In these equations u, v, w are the velocity components in *x*, *y*, *z* directions respectively, *p* is pressure, $\tau_{i,j}$ is the combination of viscous and turbulent stresses in *ij* – plane, ρ is the fluid density and *g* is acceleration due to gravity which is assumed to be 9.81 m^2/s in this study. It should be noted that overbar indicates time averaged values in these equations. Here, equation (2.1) represents the continuity equation, conserving the mass, and the equations (2.2) ~ (2.4) are the momentum conservation equations.

Numerical methods for 3D equations are very costly in large computational domains. Therefore, simplifying the equations to 2D or 1D would be more practical. In most real life cases, the flow is considered to be shallow which means the flow depth is small compared to its width. Such flows are modelled with Depth Averaged Shallow Water Equations (SWE) which can be derived by averaging the Reynolds equations

(2.1) ~ (2.4) over water depth. In this derivation the velocity component in *z*-direction (*w*) is considered to be significantly smaller than the other two components (*u*, *v*). In other words, the vertical acceleration is neglected and therefore a hydrostatic pressure distribution occurs which has linear relationship with flow depth. Thus, in the solution procedure there is no need to solve an equation for pressure. A basic sketch of a shallow free surface flow and related parameters is shown in Figure 2-1.

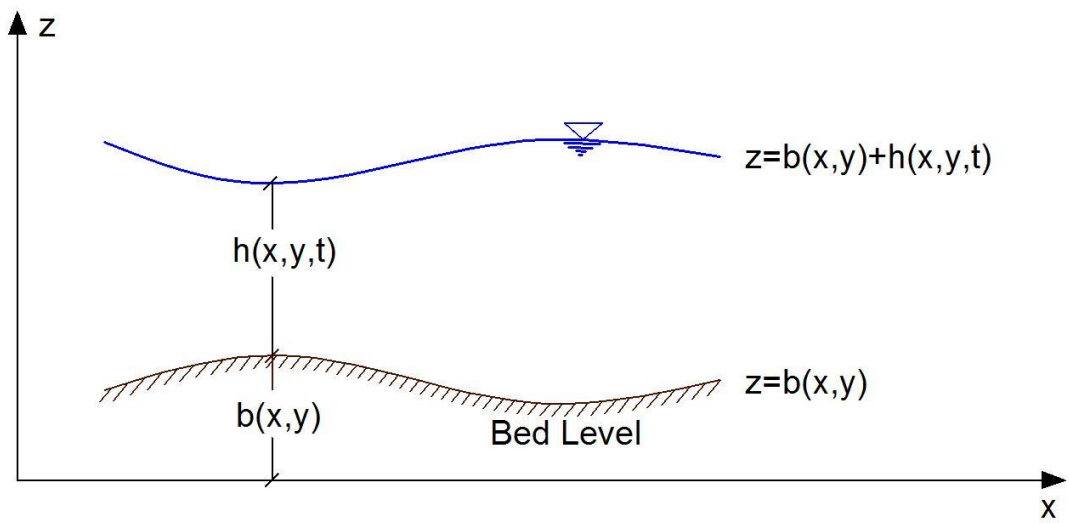

Figure 2-1 Free surface flow sketch

In this figure bed level shown as *b(x,y)*, is considered with positive elevation in *z* direction. The depth of free surface flow over this bed level is shown by *h* which is a function of *x*, *y* and *t*. The water surface boundary can be defined as the summation of the bottom boundary and flow depth.

The SWE of an incompressible and inviscid fluid in two dimensions is given by the following system of partial differential equations,

$$h_t + (hu)_x + (hv)_y = 0 \tag{2.5}$$

$$(hu)_t + (hu^2 + \frac{1}{2}gh^2)_x + (huv)_y = -ghb_x \tag{2.6}$$

$$(hv)_t + (huv)_x + (hv^2 + \frac{1}{2}gh^2)_y = -ghb_y \tag{2.7}$$

In this system of equations, (2.5) show the conservation of mass, (2.6) and (2.7) show the conservation of momentum in *x* and *y*- directions, respectively.

Now, the vector form of above equations can be written as

$$U_t + F(U)_x + G(U)_y = S(U) \tag{2.8}$$

This equation consists of three main vectors, namely vector of conserved variables (*U*), flux vectors (*F(U)* and *G(U))* and source term vector *S(U),* all of which are described as

$$U = \begin{bmatrix} h \\ hu \\ hv \end{bmatrix} \tag{2.9}$$

$$F(U) = \begin{bmatrix} hu \\ hu^2 + \frac{1}{2}gh^2 \\ huv \end{bmatrix} \tag{2.10}$$

$$G(U) = \begin{bmatrix} hv \\ hvu \\ hv^2 + \frac{1}{2}gh^2 \end{bmatrix} \tag{2.11}$$

$$S(U) = \begin{bmatrix} 0 \\ -ghb_x \\ -ghb_y \end{bmatrix} \tag{2.12}$$

The source vector may include many additional parameters such as boundary resistance, gravity force, Coriolis forces and wind forces. In this thesis, particularly, 1D SWE are studied and the source term will contain only the bottom slope, $S_0 = \frac{\partial z}{\partial x}$, as gravity component, and the friction slope, $S_f = \frac{n^2 u|u|}{h^{4/3}}$, as the boundary resistance. Here, ***n*** represents the Manning's roughness parameter. In view of equation (2.8) by dropping the parameters related to *y*-component, the 1D form of the SWE is given as

$$U_t + F(U)_x = S(U) \tag{2.13}$$

where the vectors *U*, *F* and *S* in open form are

$$U = \begin{pmatrix} h \\ q \end{pmatrix}, \quad q = hu \tag{2.14}$$

$$F = \begin{pmatrix} q \\ q.u + gh^2/2 \end{pmatrix} \tag{2.15}$$

$$S = \begin{pmatrix} 0 \\ -gh(S_0 - S_f) \end{pmatrix} = \begin{pmatrix} 0 \\ -gh(\frac{\partial z}{\partial x} - \frac{n^2 u|u|}{h^{4/3}}) \end{pmatrix} \tag{2.16}$$

It is noteworthy that the SWE are hyperbolic and non-linear equations. With the assumption of a continuous and differentiable solution for equation (2.13), the flux term, $F(U)_x$, can be expressed as $F(U)_x = F^{'}(U)(U)_x = \frac{\partial F(U)}{\partial U}\frac{\partial U}{\partial x}$. Therefore, equation (2.13) can be rewritten as

$$U_t + F^{'}(U)(U)_x = S(U) \tag{2.17}$$

And then in open form one gets

$$\begin{bmatrix} h \\ q \end{bmatrix}_t + \begin{bmatrix} 0 & 1 \\ -u^2 + gh & 2u \end{bmatrix} \begin{bmatrix} h \\ q \end{bmatrix}_x = \begin{bmatrix} 0 \\ -ghb_x \end{bmatrix} \tag{2.18}$$

In the above equation the term $F^{'}(U) = \frac{\partial F}{\partial U}$ is the Jacobian matrix of $F(U)$. In order to satisfy hyperbolic characteristic of the SWE (2.13), the coefficient matrix $F^{'}(U)$ should be diagonalizable. (Godlewski & Raviart, 1996)

Thus, for any positive flow depth *h*, the eigenvalues of the Jacobian are real numbers and can be obtained as follow

$$\lambda^1 = u - \sqrt{gh} \tag{2.19}$$

$$\lambda^2 = u + \sqrt{gh} \tag{2.20}$$

Important hyperbolic feature of SWE is that it allows information to travel as waves between one point to another in the flow system. This information is transported with a constant speed which is equal to eigenvalues in equations (2.19) and (2.20). Later on, these eigenvalues will represent the wave speeds which are vital in the solution procedure.

2.2 Numerical Schemes for 1D Depth Averaged Shallow Water Equations

2.2.1 Finite Volume Methods

The main goal in this study is to be able to deal with discontinuous solutions caused by non-linear fluxes (Alcrudo & Garcia-Navarro, 1993). Therefore, modelling the problem with SWE would be appropriate since the most important feature of these equations is the ability to cope with the discontinuities. However, the analytical solutions for these type of equations are restricted to very special cases, as a result, developing an appropriate numerical solution is essential.

During the last decades, Finite Difference (FDM) and Finite Element (FEM) methods are widely used for the solution of SWE. However, these methods produce unrealistic oscillations at discontinuities. Also, FDM do not conserve mass and require additional techniques to handle these discontinuities. Similarly, FEM conserves mass overall the domain but not in finite elements containing discontinuity. Therefore, recently numerical methods based on Finite Volume Methods (FVM) are being preferred, since FVM uses the integral form of the conservation equations on the solution domain which has been divided into finite number of cells called control volumes. In other words, mass and momentum are conserved in each control volume even when there is a discontinuity. Additionally, the flux variables can simply be simply evaluated at each cell interface by interpolating the mid-point values of neighboring cells.

In this thesis, for the solution of 1D SWE, Harten Lax and Van Leer (HLL) approach based on FVM will be utilized (Toro, 2001). It is obvious that in one dimension the domain is going to be divided into finite number of line segments (control volumes in 1D) of the form $[x_{i-1/2}, x_{i+1/2}]$.

Therefore, the first attempt to discretize the 1D shallow water equations is the integration of the governing equations defined in (2.13), over each line segment. This leads to the finite volume integral equation below

$$\int_{x_{i-1/2}}^{x_{i+1/2}} \frac{\partial}{\partial t} U(x,t)dx + \int_{x_{i-1/2}}^{x_{i+1/2}} \frac{\partial}{\partial x} F(U(x,t))dx = \int_{x_{i-1/2}}^{x_{i+1/2}} S(U(x,t))dx \tag{2.21}$$

Now, along each line segment, constant variation is assumed for the conserved variables. It means that for all $x \in [x_{i-1/2}, x_{i+1/2}]$,

$$U(x,t) \approx U(x_i,t) = U_i(t) \tag{2.22}$$

in other words,

$$\int_{x_{i-1/2}}^{x_{i+1/2}} \frac{\partial}{\partial t} U(x,t)dx \approx \frac{\partial}{\partial t} U_i(t) \int_{x_{i-1/2}}^{x_{i+1/2}} dx = \frac{\partial}{\partial t} U_i(t)\Delta x_i \tag{2.23}$$

and similarly

$$S(U(x,t)) \approx S(U_i(t)) = S_i(t) \tag{2.24}$$

where x_i is the midpoint of the interval $[x_{i-1/2}, x_{i+1/2}]$, i.e. $x_i = \frac{x_{i-1/2} + x_{i+1/2}}{2}$ and Δx_i is the length of the ith interval.

Thus, the integral equation above can be simplified as follow

$$\frac{\partial U_i(t)}{\partial t} \Delta x_i + \int_{x_{i-1/2}}^{x_{i+1/2}} \frac{\partial F(U(x,t))}{\partial x} dx = S_i(t)\Delta x_i \tag{2.25}$$

and a further simplification using Fundamental Theorem of Calculus for the flux term results in

$$\frac{\partial U_i(t)}{\partial t} \Delta x_i + \left[F(U(x_{i+1/2},t)) - F(U(x_{i-1/2},t))\right] = S_i(t)\Delta x_i \tag{2.26}$$

Then, the discretization in time direction is made by integrating equation (2.26) in time intervals $[t^n, t^{n+1}]$ of lengths Δt, i.e.

$$\int_{t^n}^{t^{n+1}} \left(\frac{\partial U_i(t)}{\partial t} \Delta x_i \right) dt + \int_{t^n}^{t^{n+1}} \left[F(U(x_{i+1/2}, t)) - F(U(x_{i-1/2}, t)) \right] dt = \int_{t^n}^{t^{n+1}} \left(S_i\,(t) \Delta x_i \right) dt \tag{2.27}$$

Now, by using the following integral averages in time for the flux terms located at the computational cell boundary,

$$F_{i-1/2}^n \approx \frac{1}{\Delta t} \int_{t^n}^{t^{n+1}} F(U(x_{i-1/2}, t)) dt \quad \text{and} \quad F_{i+1/2}^n \approx \frac{1}{\Delta t} \int_{t^n}^{t^{n+1}} F(U(x_{i+1/2}, t)) dt \tag{2.28}$$

one can rewrite the integral equation (2.27) as

$$\left[U_i(t^{n+1}) - U_i(t^n) \right] \Delta x_i + \left[F_{i+1/2}^n - F_{i-1/2}^n \right] \Delta t = S_i\,(t^n) \Delta t \Delta x_i \tag{2.29}$$

Hence, the finite volume discretization of equation (2.13), can be arranged as follow in order to give an explicit solution for U_i at the time level $t = t^{n+1}$,

$$U_i^{n+1} = U_i^n - \frac{\Delta t}{\Delta x_i} \left[F_{i+1/2}^n - F_{i-1/2}^n \right] + \Delta t S_i^n \tag{2.30}$$

In the above equation U_i^n represents the spatial average of the conserved variable at the mid-point x_i of each computational cell and time level t^n and $F_{i\pm1/2}^n$ represents the time averaged flux values located at cell boundaries (interfaces) at a time step t^n.

The principle of the finite volume method in 1D can be represented as a simple sketch in Figure 2-2 . In this figure, white dots represent the grid points and the line segments that are being divided by these dots are considered to be the control volumes. The midpoint of the computation cell is shown with black dots are control points. The conserved variables are computed for the midpoint and the flux terms are evaluated for the interface of the cell. As it is shown in Figure 2-2 , all the values are calculated in both spatial and time domains. These steps are very important in terms of accuracy, which will be discussed in more details in the following sections.

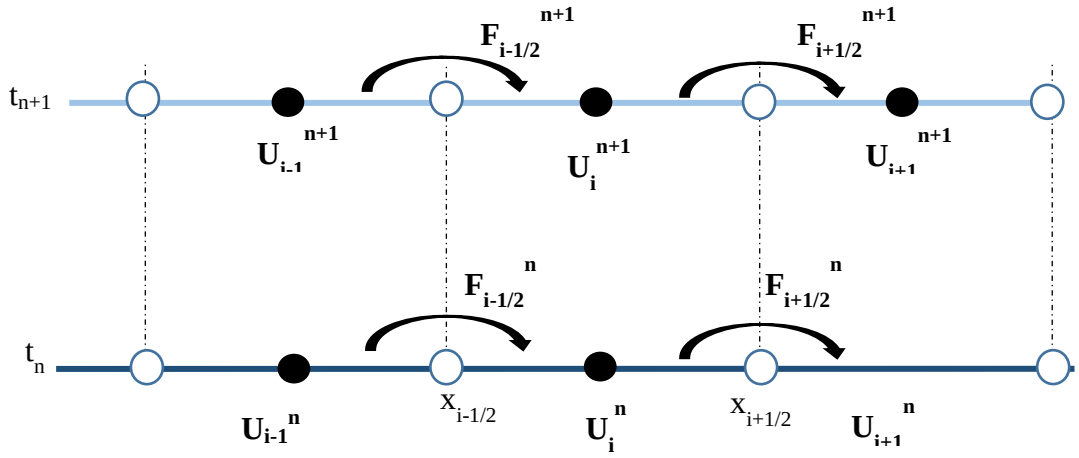

Figure 2-2 FVM solution sketch

In order to determine any of the variables in cell midpoint, a boundary condition should be specified. In this particular study upwind discretization scheme has been used which is one of the most stable discretization scheme in available numerical methods (Hussaini, Van Leer, & Van Rosendale, 1997). Primarily, this method calculates the value of each parameter at the midpoint of the cell using the upstream boundary value which has been evaluated from neighbor upstream cell indicating that the values are being calculated in the direction of the flow.

2.2.2 Approximate Riemann Solvers

The discontinuities appear on the solution of SWE, can be defined by the concept of Riemann Problem. The Riemann problem is a one dimensional initial value problem which has been introduced to solve a set of conservation laws described by hyperbolic equations. This problem can be considered as a generalization of the dam break problem. It shows the initial values of the problem which are discontinuous at distance *x*. The Riemann problem can be shown as

$$U_t + F_x(U) = 0 \tag{2.31}$$

$$U(x,0) = \begin{cases} U^L & if \quad x < 0 \\ U^R & if \quad x > 0 \end{cases} \tag{2.32}$$

There are numerous methods available in the literature to solve Riemann Problem which can be either exact or approximate. Being complex and time consuming and having high computational cost are some of the Exact Riemann solvers drawbacks. Approximate Riemann solvers on the other hand, are easier to conduct as well as being cheaper and faster compared to the exact solutions. According to Toro, (Toro, 2001) approximate Riemann solvers can save up to 20 % in cost compared to exact solution. Aside from these advantages the correctness and accuracy of the method is the most important criteria, since the approximate Riemann solvers give quite accurate results, consequently, these methods have become more popular and preferable by researchers. Some of the most popular approximate Riemann solvers are Godunov's method with Roe averaging, Osher's method, HLL and Weighted Average Flux (WAF).

The general structure of Riemann problem solution can be represented in *x*-*t* plane. The solution consists of several waves each of which represent a distinct real number of eigenvalues and as it was mentioned before, they have an important role in the transportation of the discontinuity between computational cells.

These waves may occur as shock waves, rarefactions and shear wave. A general view of the speeds and possible locations of these waves can be seen in Figure 2-3 and they can be classified with the superscripts *L*, *R* and *. Here, λ^L and λ^R will be either shock waves or rarefactions and in the area between these two waves, called as the star region, there may occur shear waves, λ^*, showing the discontinuity location. The shear wave itself has the speed of *u* and in order to define the speeds of wave propagation (λ^L and λ^R), a parameter named Celerity is described

$$c = \sqrt{gh} \tag{2.33}$$

Note that this equation is only valid for SWE when the ratio of water depth to wave length is less than 0.05 (Sorensen, 1993).

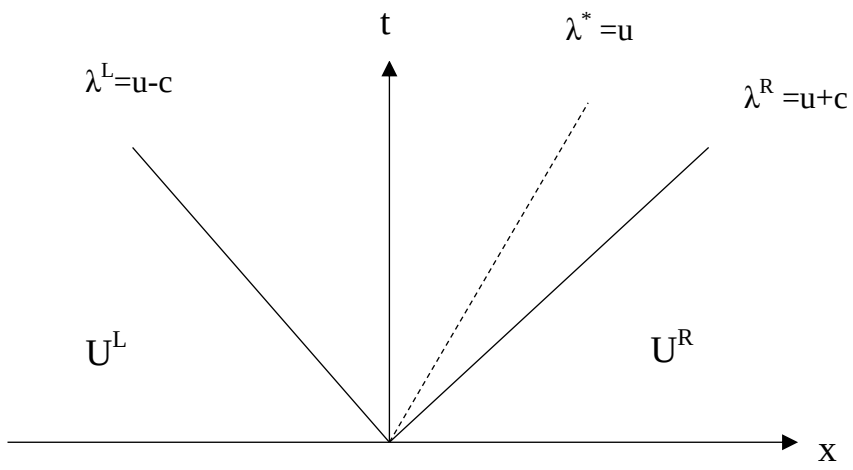

Figure 2-3 The solution of Riemann problem

It is well known that, a good example for Riemann problem is the classic 1D dam break problem which can be seen geometrically in Figure 2-4 in detail. When the transition is smooth and increasing in the opposite direction of the flow, the wave is known as a rarefaction. On the other hand, if the characteristic family decreases in the flow direction abruptly, the separating wave is called as a shock wave. There are several possible combinations of these shocks or waves which depend on the initial condition of the problem. The solutions for the regions at the left of λ^L and right of λ^R remains the same as the initial condition given in equation (2.32), since the characteristic information has not being reached those areas yet (Toro, 2001).

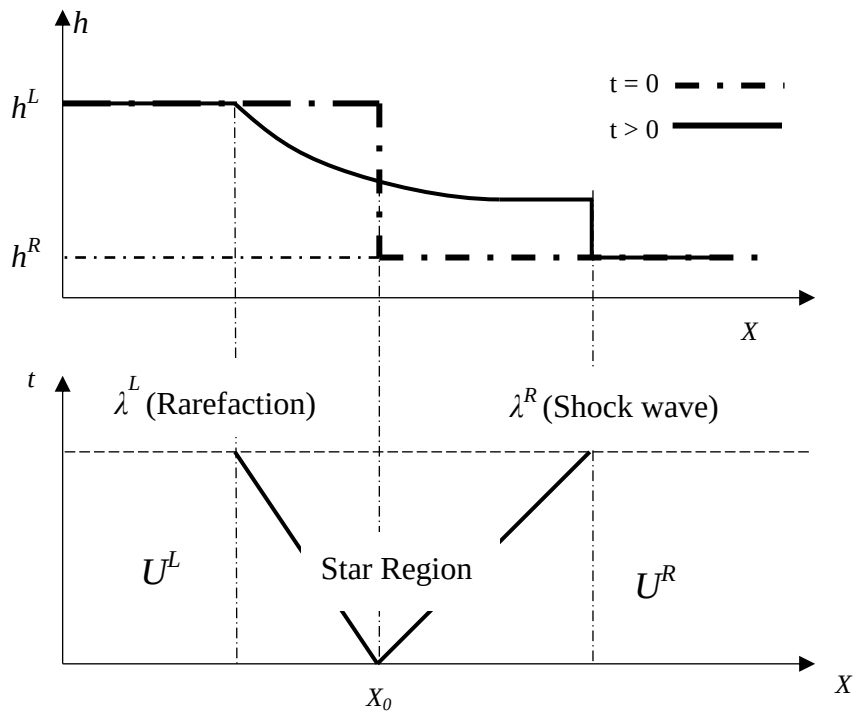

Figure 2-4 A geometrical sketch of dam break problem

All the available numerical methods are generally based on solving the Riemann problem at interfaces between control volumes. In the solution procedure, the conserved variables are assumed to be constant along each line segment. Thus, this may produce discontinuity between cells. In order to overcome these discontinuities, the numerical method should take into account the flow direction while approximating the interface flux values. In other words, this upwind feature of the method will allow discontinuous solutions. However, the flux approximation at interfaces makes the difference between these methods (Toro, 2009). For instance, the Godunov's Upwind Method solves the Riemann problem at each interface by making use of Roe’s averages for the flux approximation. A general description of this method is shown in Figure 2-5. First, in part (a) the computation of flux values are shown at each cell interface, second the assumption of piecewise constant data construction is presented and in (c) the local Riemann problem at each interface can be seen.

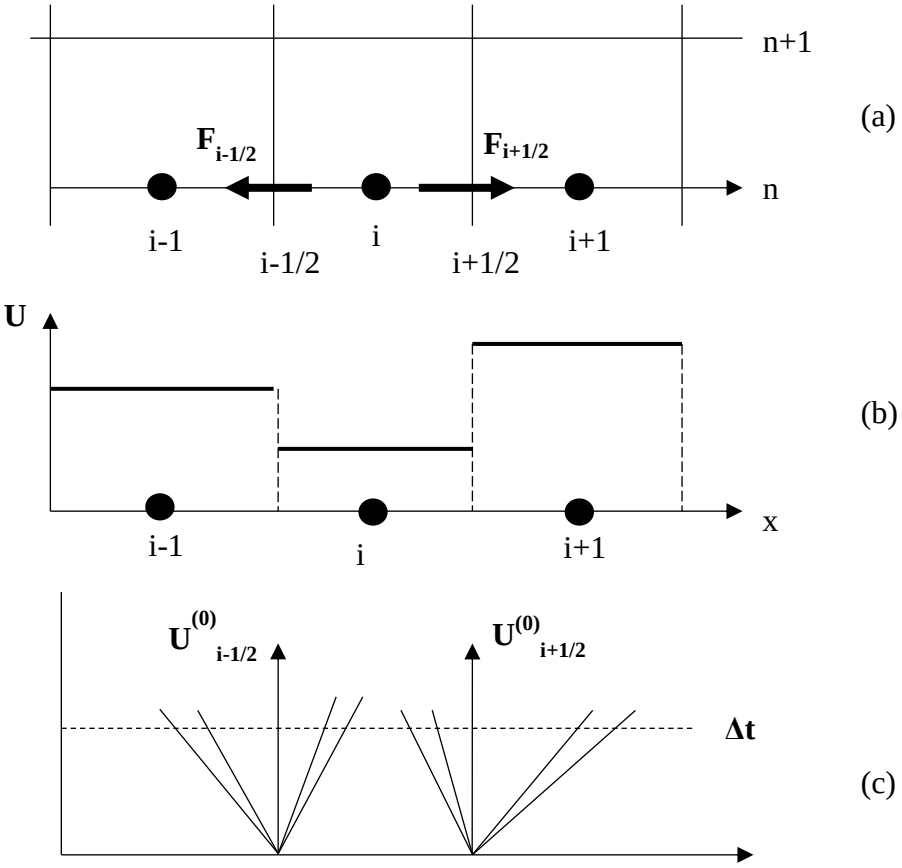

Figure 2-5 Godunov's upwind method for 1D flow: (a) Control volume in x-t space, (b) Integral averages giving piecewise constant data,(c) Structure of the solution of Riemann problem at interfaces (Toro, 2001)

A special case of dam break problem is considered (Figure 2-4) where there is only water accumulated behind the gate but the bed is dry at the front, which means the value for h^R is equal to zero. In this case, the two eigenvalues will overlap, making the SWE not hyperbolic anymore. Thus the method will lose its shock capturing ability. In literature there exists two well-known approximate Riemann solvers which are able to solve the dry bed case problem directly. These two methods are HLL and Weighted Average Flux (WAF) scheme (Zoppou & Roberts, 2003). In this thesis, HLL approximate Riemann solver is preferred for simplicity in 1D solutions.

2.2.3 HLL Approach

First order HLL approximate Riemann solver was introduced by Harten Lax and van Leer in 1983 (Toro, 2009). This approximate Riemann solver only considers the fastest waves, namely λ^L and λ^R, as an estimation for the smallest and largest wave speeds in the solution of the Riemann problem (Figure 2-6) (Murawski, Murawski, & Stpiczynski, 2012). At the interface, *i+1/2,* for the left (L) and right (R) states of the conserved variables, the following assumptions are made

$$U^L \equiv U_i^n \ , \ \ U^R \equiv U_{i+1}^n \tag{2.34}$$

with the corresponding flux values

$$F^L \equiv F(U^R) \, , \ F^R \equiv F(U^R) \tag{2.35}$$

Note that, here, the intermediate waves, such as shear waves or contact discontinuities are omitted based on this approach and thus a two wave Riemann solution is achieved.

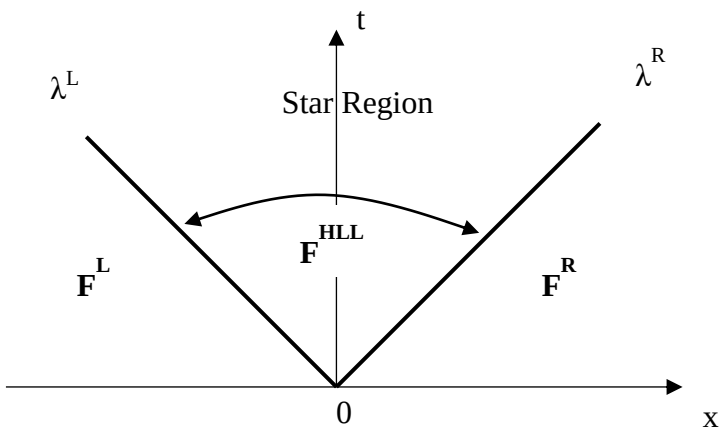

Figure 2-6 Two-wave Riemann solution structure for HLL method (Toro, 2001)

The HLL approximation used in the computation of flux values appearing in the discretized equation (2.30) has the following form (Toro, 2001)

$$F_{i+1/2}^{HLL} = \begin{cases} F_{i+1/2}^{L} & if \quad 0 \le \lambda^{L} \\ \dfrac{\lambda^{R} F^{L} - \lambda^{L} F^{R} + \lambda^{L}\lambda^{R}(U^{R} - U^{L})}{\lambda^{R} - \lambda^{L}} & if \quad \lambda^{L} \le 0 \le \lambda^{R} \\ F_{i+1/2}^{R} & if \quad 0 \ge \lambda^{R} \end{cases} \tag{2.36}$$

Here, without loss of generality, the HLL flux treatment is described for the interface at *i+1/2* location.

As stated, the presented HLL method is first order accurate with the assumptions (2.34) and (2.35) in which the right and left state contributions only come from the two adjacent cells, *i* and *i+1*. In order to increase the order of accuracy, the MUSCL – Hancock scheme (Toro, 2001) is made use of in space and time. Further, for the expected oscillations at discontinuities, the MUSCL – Hancock scheme process is improved by using a Total Variation Diminishing (TVD) approach based on limiting the slopes of conserved variables.

Note that, in HLL approach shear waves are ignored. However, in literature, there exists a modified version of it called HLLC scheme, which also covers the shear waves and the contact discontinuities. Thus, the HLLC solver structure implies a three wave Riemann solution as in Figure 2-7 and it is more suitable for 2D problems.

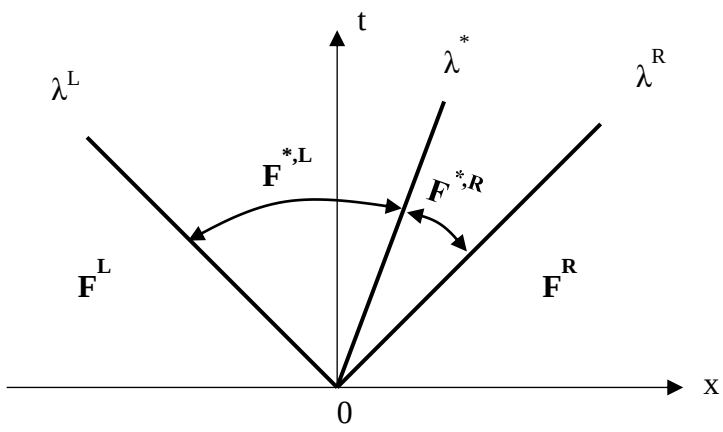

Figure 2-7 Three-wave Riemann solution structure for HLLC method (Toro, 2001)

In this thesis, the HLL solution of one dimensional problems and their applications will be considered. A detailed interpretation about the improvement of HLL approach with TVD and MUSCL – Hancock is given in sections 2.2.4 and 2.2.5.

2.2.4 MUSCL – Hancock Approach (Variable Extrapolation Approach)

The ideal numerical method is the one giving the solutions with higher accuracy and lower error. Van Leer introduced the MUSCL (Monotone Upstream-Centered Scheme) or Variable Extrapolation approach in order to modify the first order schemes (Van Leer, 1977). Later on, the original MUSCL method was modified by Steve Hancock, a fluid mechanics graduate student of UC Berkeley University, in which one achieves second order accuracy in both space and time (Van Leer, 2006).

The MUSCL-Hancock method involves three steps; data reconstruction, the boundary value evaluation and determination of flux values at interfaces using approximate Riemann solver.

Firstly, a piecewise linear reconstruction of conserved variables in computational cell, i, is considered, (Figure 2-8). Here the piecewise linear function $U_i(x)$ will replace the previously assumed piecewise constant data U_i^n.

$$U_i(x) = U_i^n + \frac{(x - x_i)}{\Delta x}\Delta U_i \ , \ x \in [0, \Delta x] \tag{2.37}$$

In this equation, $\frac{\Delta U_i}{\Delta x}$ is the slope of $U_i(x)$ in the computational cell, *i*, and x_i, shows the midpoint of the cell. As the second step, the necessary right and left contributions for interface values are given with equations (2.38)

$$U_i^L = U_i^n - \frac{1}{2}\Delta U_i \ , \ U_i^R = U_i^n + \frac{1}{2}\Delta U_i \tag{2.38}$$

These boundary extrapolated values, are used in the solution of local Riemann problem at every discontinuous point.

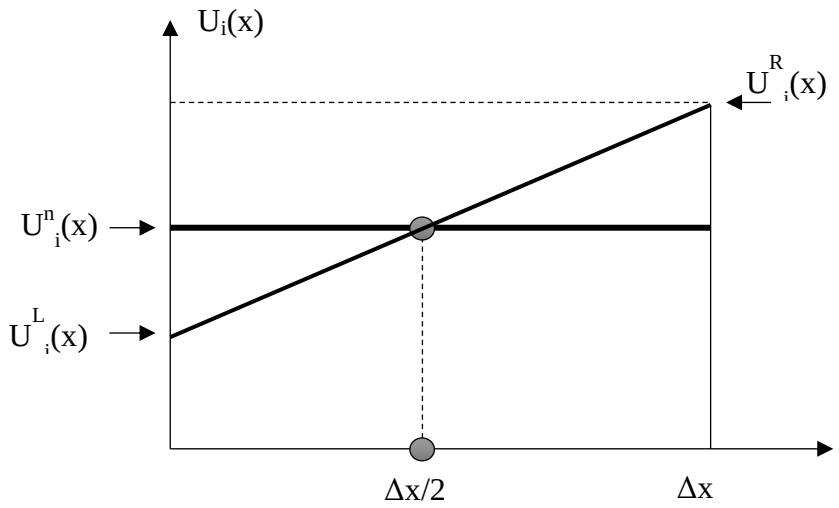

Figure 2-8 Piecewise linear MUSCL reconstruction of data in a single cell, i (Toro, 2009)

Now, writing ΔU_i in a more general form, would result in an equation which includes differentiable extrapolations at the cell interfaces

$$\Delta \mathrm{U}_{\mathrm{i}} = \frac{1}{2}\left[(1+\omega)\Delta \mathrm{U}_{\mathrm{i-1/2}} + (1-\omega)\Delta \mathrm{U}_{\mathrm{i+1/2}}\right] \tag{2.39}$$

where

$$\Delta \mathrm{U}_{\mathrm{i+1/2}} = U_{i+1}^{n} - U_{i}^{n}, \;\; \Delta \mathrm{U}_{\mathrm{i-1/2}} = U_{i}^{n} - U_{i-1}^{n} \tag{2.40}$$

and ω is a free parameter between [-1,1].

Next, the extrapolated conserved variables at cell interfaces, such as at *i+1/2*, are obtained as follow (Figure 2-9)

$$U_{i+1/2}^{L} = U_{i} + \frac{1}{2}\Delta U_{i-1/2} \tag{2.41}$$

$$U_{i+1/2}^{R} = U_{i+1} - \frac{1}{2}\Delta U_{i+1/2} \tag{2.42}$$

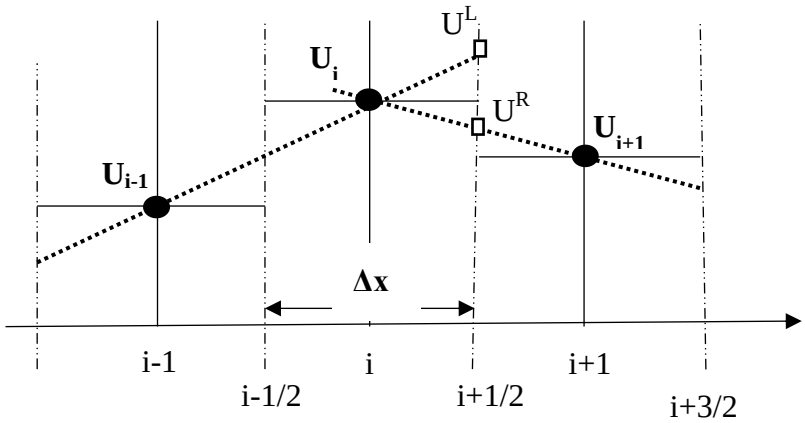

Figure 2-9 MUSCL-Hancock method representation (Zoppou & Roberts, 2003)

For the last step of MUSCL-Hancock approach, the values for interface fluxes is obtained according to HLL approximate Riemann solver given in equation (2.36). More detailed information about the application of this approach during the discretization process in order to have higher order accuracy in time, will be given in chapter 3.

As it was mentioned, these higher order extensions would result in spurious oscillations at the cell interfaces. Thus, to overcome this deficiency, TVD limitation will be applied on MUSCL approach, which is going to be discussed in the next section.

2.2.5 High-Resolution Schemes

As stated, there exist two main deficiencies regarding the basic first order numerical methods; inaccuracies due to their low order of accuracy and unrealistic oscillations at discontinuities. However, by making use of MUSCL-Hancock extrapolation method, the order of accuracy for the numerical scheme can be increased. Additionally, total variation diminishing schemes have been developed specifically to eliminate the unwanted oscillations. TVD is actually a property which is applied to discretization of SWE to treat these oscillations by adding or subtracting artificial dissipative amount in the flow direction (Versteeg & Malalasekera, 2007).

Considering a discrete solution as shown in Figure 2-10, the total variation can be defined as follow

$$TV(U) = |U_2 - U_1| + |U_3 - U_2| + |U_4 - U_3| \tag{2.43}$$

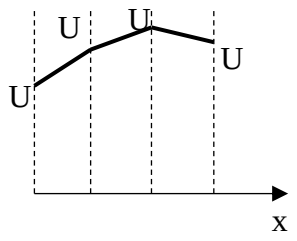

Figure 2-10 Explanation of total variation concept

The role of TVD can be defined in this concept, where with monotonicity-preserving property the total variation of this discrete solution would be diminished with time.

According to Sweby (1984) there are some conditions where the scheme should be met for it to be TVD and these conditions are defined in terms of two parameters r and ψ. The parameter r is a ratio of upwind difference to local difference of the conserved variable and ψ is called the limiting function which does the diminishing of the oscillations and is a function of a common parameter (r).

In recent years a number of limiters have been proposed in the literature and the most commonly used ones are shown in Table 2-1 .

Table 2-1 Slope limiter functions (Versteeg & Malalasekera, 2007)

Name	Limiter Function ψ (r)	Source
Van Leer	$\frac{r+\lvert r\rvert}{1+r}$	Van Leer(1974)
Van Albada	$\frac{r+r^2}{1+r^2}$	Van Albada et al. (1982)
Min-Mod	$\begin{cases} \min(r,1) & if \quad r>0 \\ 0 & if \quad r \le 0 \end{cases}$	Roe (1985)
SUPERBEE	$\max[0, \min(2r,1), \min(r,2)]$	Roe (1985)
Sweby	$\max[0, \min(\beta,1), \min(r,\beta)]$	Sweby (1984)
QUICK	$\max[0, \min(2r, \frac{3+r}{4}, 2)]$	Leonard (1988)

UMIST	$\max[0, \min(2r, \frac{1+3r}{4}, \frac{3+r}{4}, 2)]$	Lien and Leschziner (1993)

The graph of these limiter are visualized in Figure 2-11 for $r \in [0,8]$. One of the important criteria for a stable TVD scheme introduced by Sweby is that for a limiter function to be 2nd order accurate, it should pass through point (1,1). As it is shown in Figure 2-11, all the mentioned limiters are passing through this point which states their 2nd order accuracy. Moreover, the only smooth limiter functions in this figure are Van Leer and Van Albada and the other limiters have piecewise structure. In the acceptable TVD region, which is shown by gray filling, the lower limit is Min-Mod and the upper limit is shown by SUPERBEE limiter functions. This shows that the Min-Mod limiter function is the most dissipative among these functions (Murillo & Garcia-Navarro, 2012). The generalization of SUPERBEE and Min-Mod limiter is named as Sweby's limiter and an additional parameter has been defined here as β. For β values between 1 and 2 these limiters stay in TVD region. All these limiter functions have different characteristics which may affect the results of the numerical method.

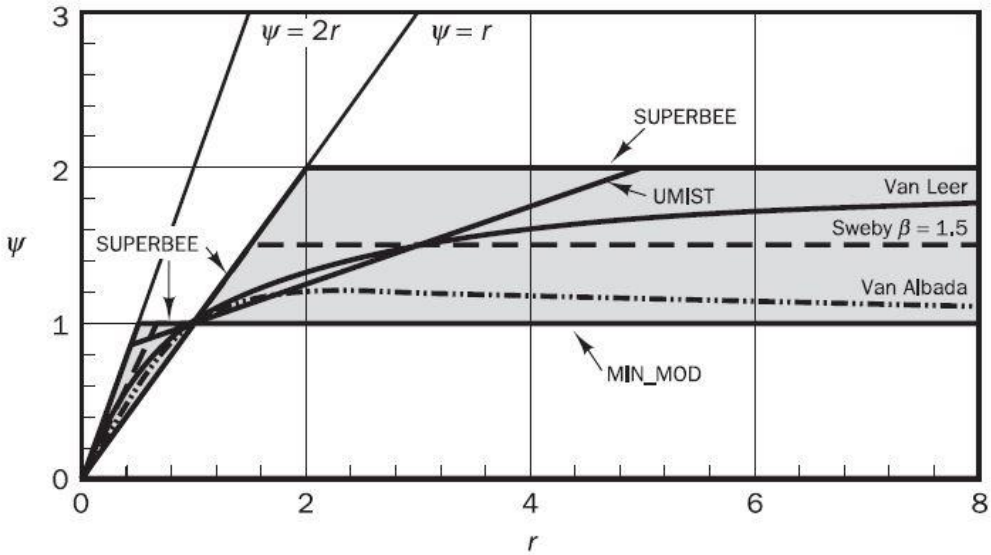

Figure 2-11 Limiter function comparison (Versteeg & Malalasekera, 2007)

As previously stated, in order to eliminate the unrealistic oscillations, the reconstructed slopes in MUSCL approach are limited with a slope limiter function. (Anastasiou & Chan, 1997). By applying one of the limiter functions above, the values of conserved variables at the interface *i+1/2*, become

$$U_{i+1/2}^{L} = U_i + \frac{1}{2}\psi(r_{i+1/2})\Delta U_{i-1/2} \tag{2.44}$$

$$U_{i+1/2}^{R} = U_{i+1} - \frac{1}{2}\psi(r_{i+1/2})\Delta U_{i+1/2} \tag{2.45}$$

Then, these boundary values are used in computing the flux terms at the interface of the cell (Alias, Liang, & Kesserwani, 2011). In the next chapter, a general view of discretization of 1D SWE with the application of TVD based MUSCL-Hancock is given and the algorithm of the scheme is discussed in detail.

CHAPTER 3

NUMERICAL METHOD ADOPTED TO PRESENT PROBLEM

3.1 Discretization of the 1D SWE Equations using HLL Numerical Scheme

Let us recall the one dimensional shallow water equation (equation (2.13))

$$\frac{\partial U}{\partial t} + \frac{\partial F(U)}{\partial x} = S(U)$$

with the following open form described in equations (2.14) ~ (2.16)

$$\begin{pmatrix} h \\ q \end{pmatrix}_t + \begin{pmatrix} q \\ q.u + gh^2/2 \end{pmatrix}_x = \begin{pmatrix} 0 \\ -gh(\frac{\partial z}{\partial x} - \frac{n^2 u|u|}{h^{4/3}}) \end{pmatrix}$$

and also recall the general FVM discretization (equation (2.30)) derived in Section 2.2.1 for 1D SWE

$$U_i^{n+1} = U_i^n - \frac{\Delta t}{\Delta x}[F_{i+1/2}^n - F_{i-1/2}^n] + \Delta t.S_i^n$$

This formula is first order in time and space but it turns out to be second order accurate in space when the flux terms are approximated by the HLL approach, $F_{i\pm 1/2}^n \approx F_{i\pm 1/2}^{HLL,n}$ (equation(2.36)), in which the conserved variables are reconstructed by using a TVD version of MUSCL-Hancock extrapolation . Accordingly, the finite volume statement above can be rewritten as in equation (3.1) within the HLL flux approximations in order to gain the shock capturing property and higher order accuracy

$$U_i^{n+1} = U_i^n - \frac{\Delta t}{\Delta x}[F_{i+1/2}^{HLL,n} - F_{i-1/2}^{HLL,n}] + \Delta t S_i^n \qquad (3.1)$$

Equation (3.1) is second order in space as the fluxes are obtained at mid points between the computational grid nodes. Now, second order accuracy also in time is achieved by splitting the solution into two time steps. At first, a half time step $\Delta t/2$

is used, called Predictor Step, where all the dependent variables at time level $t^{n+1/2}$ are determined from the values at the time level t^n. Then, a full time step (Δt) is used, called the Corrector Step, again all the parameters are being calculated using the predictor step values. This Predictor-Corrector algorithm was suggested in MUSCL-Hancock approach (Alcrudo & Garcia-Navarro, 1993) and is stated from Equation (3.1) as

The Predictor Step

$$U_i^{n+1/2} = U_i^n - \frac{\Delta t}{2\Delta x}[F_{i+1/2}^{HLL,n} - F_{i-1/2}^{HLL,n}] + \frac{\Delta t}{2} S_i^n \tag{3.2}$$

The Corrector Step

$$U_i^{n+1} = U_i^n - \frac{\Delta t}{\Delta x}[F_{i+1/2}^{HLL,n+1/2} - F_{i-1/2}^{HLL,n+1/2}] + \Delta t S_i^{n+1/2} \tag{3.3}$$

It should be noted that the superscript shown next to the variables indicates the time step or it determines which side of the computed cell the variable is located at (right/left) and the subscript indicates the spatial location of the evaluated parameter.

In the solution, the right and left approximations of the interface values of variables are required which can be obtained by using MUSCL approach. However, the variations of any dependent variable may give spurious oscillations in the solution. To avoid unphysical oscillations and keep stability of numerical solution limiter function will be used as slope limiters for dependent variables. As it was explained in section 2.2.4, slope limiter is a function of a parameter named (*r*). The parameter, *r* is the ratio of upwind difference to central difference and functions as a switch to determine the flow direction. The velocity component in *x*-direction for the right face of the ith cell (Figure 3.1)vis calculated by averaging

$$u_i^{Interface} = (u_i + u_{i+1})/2 \tag{3.4}$$

The characteristic wave speed for the face of the cell can be obtained by finding the interface water depth and celerity

$$h_i^{Interface} = (h_i + h_{i+1})/2 \tag{3.5}$$

$$c_i^{Interface} = \sqrt{g h_i^{Interface}} \tag{3.6}$$

Then, the wind direction is

$$WD_i = u_i^{Interface} - c_i^{Interface} \tag{3.7}$$

If $WD>0$

$$\Delta U_{upwind} = h_{i+1} - h_{i+2} \tag{3.8}$$

$$\Delta U_{Local} = h_i - h_{i+1} \tag{3.9}$$

If $WD<0$

$$\Delta U_{upwind} = h_i - h_{i-1} \tag{3.10}$$

$$\Delta U_{Local} = h_{i+1} - h_i \tag{3.11}$$

The parameter r is then obtained from

$$r_{i+1/2} = \frac{\Delta U_{upwind}}{\Delta U_{Local}} \tag{3.12}$$

Using the r ratio and one of the slope limiter functions from Table 2-1 , limited variations of flow quantities can be evaluate

$$\delta U_i^n = (U_i^n - U_{i-1}^n)\psi(r_U) \tag{3.13}$$

$$U_{i+1/2}^R = U_{i+1}^n - \frac{1}{2}(\delta U)_{i+1}^n \tag{3.14}$$

$$U_{i+1/2}^L = U_i^n + \frac{1}{2}(\delta U)_i^n \tag{3.15}$$

where ψ is the limiter function. Using the interface values obtained, one can determine the interface fluxes for HLL method using equation (2.36) (Alias, Liang, & Kesserwani, 2011).

Considering the grid system shown in Figure 3.1 , the above general algorithm should be repeated for continuity and momentum equation separately. Writing these equations individually, we get

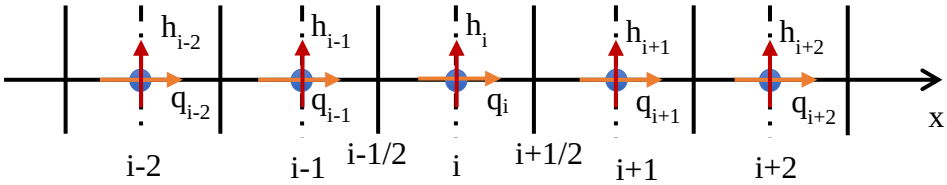

Figure 3.1 The grid system in 1D solution

- **Continuity Equation**

$$\frac{\partial h}{\partial t}+\frac{\partial(q)}{\partial x}=0 \tag{3.16}$$

- **Momentum Equation**

$$\frac{\partial(q)}{\partial t}+\frac{\partial(qu+gh^2/2)}{\partial x}=-gh(\frac{\partial z}{\partial x}-\frac{n^2u|u|}{h^{4/3}}) \tag{3.17}$$

As it was mentioned before, all the variables will be computed in two half time step. In the predictor step the values will be determined by using the previous full time step values, and in the corrector step, results of predictor step will be used. This loop would repeat and the values will be updated till the desired condition has been reached.

Calculating the slope limiters and intermediate boundary extrapolated values for both continuity and momentum at predictor step would be as follow

Continuity $$(\delta h)_i^n=(h_i^n-h_{i-1}^n)\psi(r_h) \tag{3.18}$$

Momentum $$(\delta q)_i^n=(q_i^n-q_{i-1}^n)\psi(r_q) \tag{3.19}$$

Next, the intermediate values at computation cells would be determined again for both equations as below

Continuity

$$h_{i+1/2}^R=h_{i+1}^n-\frac{1}{2}(\delta h)_{i+1}^n \tag{3.20}$$

$$h_{i+1/2}^{L} = h_i^n + \frac{1}{2}(\delta h)_i^n \tag{3.21}$$

Momentum

$$q_{i+1/2}^{R} = q_{i+1}^n - \frac{1}{2}(\delta q)_{i+1}^n \tag{3.22}$$

$$q_{i+1/2}^{L} = q_i^n + \frac{1}{2}(\delta q)_i^n \tag{3.23}$$

It should be noted that, the main parameters in this problem are h and $q = hu$, thus, the value of velocity can be simply calculated from

$$u_{i+1/2}^{R} = \frac{q_{i+1/2}^{R}}{h_{i+1/2}^{R}} \tag{3.24}$$

$$u_{i+1/2}^{L} = \frac{q_{i+1/2}^{L}}{h_{i+1/2}^{L}} \tag{3.25}$$

Next step is to evaluate the flux terms for both continuity and momentum equation separately according to the speed of wave in the computational cell.

For each wave region (left, right and star), there exists a distinct flux equation. According to Toro (Zia & Banihashemi, 2008), in order to use the HLL method correctly it is essential to identify the proper wave. In order to do so, firstly, the values of velocity and depth at the star region, u^* and h^*, are computed from equations below

$$u^* = \frac{(u^L + u^R)}{2} + \sqrt{gh^L} - \sqrt{gh^R} \tag{3.26}$$

$$h^* = \frac{(u^L + 2\sqrt{gh^L} - u^R + 2\sqrt{gh^R})^2}{16g} \tag{3.27}$$

Here h^k and u^k represent the initial values for a local Riemann problem with k=L, R.

Although there are lots of possibilities for the combination of these waves, Toro suggests the following three general cases are sufficient for covering majority of

possibilities (Zia & Banihashemi, 2008). These cases include, shock wave, rarefaction and the special case of dry bed. Wave speeds for each case can be obtained as follow

- In case of shock

$$\begin{aligned} \lambda^L &= u^L - \sqrt{gh^L}\, q^L \\ \lambda^R &= u^R + \sqrt{gh^R}\, q^R \end{aligned} \quad \text{if} \quad h^* > h^k \tag{3.28}$$

Here, q represents the unit discharge value and it can be defined as follow

$$q^k = \sqrt{\frac{1}{2}\left[\frac{(h^* + h^k)h^k}{(h^k)^2}\right]} \tag{3.29}$$

- In case of rarefaction wave

$$\begin{aligned} \lambda^L &= \min(u^L - \sqrt{gh^L}, u^* - \sqrt{gh^*}) \\ \lambda^R &= \max(u^R + \sqrt{gh^R}, u^* + \sqrt{gh^*}) \end{aligned} \quad \text{if} \quad h^* \le h^k \tag{3.30}$$

- In case of dry bed (which is out of the scope of this study but is included in the code for further studies)

$$\begin{aligned} \lambda^L &= u^R - 2\sqrt{gh^R} \quad \text{for } h^L = 0 \\ \lambda^R &= u^L + 2\sqrt{gh^L} \quad \text{for } h^R = 0 \end{aligned} \tag{3.31}$$

The values for intermediate fluxes at the face of the cell would be defined as follow

- Flux terms for continuity equation:

$$FC^R_{i+1/2} = q^R_{i+1/2} \tag{3.32}$$

$$FC^L_{i+1/2} = q^L_{i+1/2} \tag{3.33}$$

$$FC_{i+1/2}^{HLL} = \begin{cases} FC_{i+1/2}^{L} & if \quad 0 \le \lambda^{L} \\ \dfrac{\lambda^{R}(FC_{i+1/2}^{L}) - \lambda^{L}(FC_{i+1/2}^{R}) + \lambda^{L}\lambda^{R}(h_{i+1/2}^{R} - h_{i+1/2}^{L})}{\lambda^{R} - \lambda^{L}} & if \quad \lambda^{L} \le 0 \le \lambda^{R} \\ FC_{i+1/2}^{R} & if \quad 0 \ge \lambda^{R} \end{cases}$$

(3.34)

- Flux term for momentum equation:

$$FM_{i+1/2}^{R} = q_{i+1/2}^{R} * u_{i+1/2}^{R} + \frac{g}{2} * (h_{i+1/2}^{R})^{2} \tag{3.35}$$

$$FM_{i+1/2}^{L} = q_{i+1/2}^{L} * u_{i+1/2}^{L} + \frac{g}{2}(h_{i+1/2}^{L})^{2} \tag{3.36}$$

$$FM_{i+1/2}^{HLL} = \begin{cases} FM_{i+1/2}^{L} & if \quad 0 \le \lambda^{L} \\ \dfrac{\lambda^{R}(FM_{i+1/2}^{L}) - \lambda^{L}(FM_{i+1/2}^{R}) + \lambda^{L}\lambda^{R}(q_{i+1/2}^{R} - q_{i+1/2}^{L})}{\lambda^{R} - \lambda^{L}} & if \quad \lambda^{L} \le 0 \le \lambda^{R} \\ FM_{i+1/2}^{R} & if \quad 0 \ge \lambda^{R} \end{cases}$$

(3.37)

The last step is to calculate the value of conserved variables for predictor step

$$h_{i}^{n+1/2} = h_{i}^{n} - \frac{\Delta t}{2\Delta x}[FC_{i+1/2}^{HLL,n} - FC_{i-1/2}^{HLL,n}] \tag{3.38}$$

$$q_{i}^{n+1/2} = q_{i}^{n} - \frac{\Delta t}{2\Delta x}[FM_{i+1/2}^{HLL,n} - FM_{i-1/2}^{HLL,n}] + \frac{\Delta t}{2}(gh_{i}^{n}(\frac{z_{i+1} - z_{i-1}}{x_{i+1} - x_{i-1}} - \frac{n^{2}u_{i}^{n}\left|u_{i}^{n}\right|}{(h_{i}^{n})^{4/3}})) \tag{3.39}$$

All these steps should be repeated with the new values of the variables obtained from predictor step

$$h_{i}^{n+1} = h_{i}^{n} - \frac{\Delta t}{\Delta x}[FC_{i+1/2}^{HLL,n+`1/2} - FC_{i-1/2}^{HLL,n+`1/2}] \tag{3.40}$$

$$q_{i}^{n+1} = q_{i}^{n} - \frac{\Delta t}{\Delta x}[FM_{i+1/2}^{HLL,n+1/2} - FM_{i-1/2}^{HLL,n+1/2}] + \Delta t(gh_{i}^{n+1/2}(\frac{z_{i+1} - z_{i-1}}{x_{i+1} - x_{i-1}} + \frac{n^{2}u_{i}^{n+1/2}\left|u_{i}^{n+1/2}\right|}{(h_{i}^{n+1/2})^{4/3}}))$$

(3.41)

3.2 Initial and Boundary Conditions

Initial condition for all the cases that have been studied so far in this thesis, is two different stationary water levels with an imaginary gate in between. On the left side of the gate the water level is high and on the right hand side of the gate the water level is low. At first, the variable q is equal to zero everywhere since there is no flow at t=0.

Boundary conditions play an important role in the result of the solution of any problem. In all of the cases, the domain is divided into M control volumes (line segments). In order to define appropriate boundary conditions three ghost cells are added to M, namely $i=0$, $M+1$ and $M+2$. (Figure 3.1 At the wall boundaries a normal reflective boundary condition is imposed. For the velocity

$$u_0 = -u_1 \tag{3.42}$$

$$u_{M+1} = -u_M \tag{3.43}$$

$$u_{M+2} = -u_{M-1} \tag{3.44}$$

Having the midpoint velocity in two consecutive computational cell equal with opposite sign is another way to imply the velocity at the interface of the cell as zero. This type of boundary condition is known as Neumann type boundary condition, in which the normal gradient of the variable is being introduced to the solution. For water depth the boundary condition would become

$$h_0 = h_1 - S_{0,1}\Delta x \tag{3.45}$$

$$h_{M+1} = h_M + S_{0,M}\Delta x \tag{3.46}$$

$$h_{M+2} = h_{M+1} + S_{0,M+1}\Delta x \tag{3.47}$$

By applying this condition to both sides of the closed domain, although there were no inflow/outflows, a decrease/increase in total volume of flow was observed. The problem with this condition is that Neumann type boundary condition cannot be applied on both sides at the same time. Therefore, one of the parameters should be fixed at one end. Considering the fact that the total volume should remain constant, a

specific boundary condition has been applied on one of the walls. Calculating the initial volume of fluid in the closed domain, and equating this value to the computed volume at the end of each corrector step, the value for water depth is calculated for the last cell in the domain.

$$V = \sum_{i=1}^{i=M} h_i * \Delta x \tag{3.48}$$

$$V_{Initial} = V_{Final} = \left[\sum_{i=1}^{i=M-1} h_i * \Delta x \right] + h_m \Delta x = V_{Final}^{*} + h_m \Delta x \tag{3.49}$$

The fixed value of water depth at the end wall is calculated from

$$h_m = \frac{V_{initial} - V_{Final}^{*}}{\Delta x} \tag{3.50}$$

Using equation (3.50) the value for water depth can be updated for the last computational cell, then applying the boundary condition shown in equations (3.45) ~ (3.47) would give accurate results. The ghost cell values for q can be simply calculated by the equation below

$$q = hu \tag{3.51}$$

3.3 Stability Criteria

All of the numerical methods may introduce some computational errors. For a numerical method to be considered appropriate and stable, errors occurring in the algorithm should not have major effect on the final result, meaning it should not grow throughout the solution. It is crucial to observe whether the method is stable or not. The stability condition for the 2D SWE is proposed as (Alcrudo & Garcia-Navarro, 1993)

$$\Delta t \leq \frac{\min\{\Delta x_{i,j}\}}{2\max\left\{\left(c + \sqrt{\left[u^2 + v^2\right]}\right)_{i,j}\right\}} \tag{3.52}$$

where Δx, shows the distance between midpoints of computational cells and c is celerity. For the present 1D solution, it is adopted as

$$\Delta t = CFL * \frac{\Delta x}{\max(0, \sqrt{g * h_i} + |u_i|)} \tag{3.53}$$

where CFL (Courant-Friedrichs-Levy) number is fixed as 0.9 after a series of numerical tests. Time step size (Δt) was calculated for each cell at every time step and the minimum value was used in the solution.

CHAPTER 4

NUMERICAL SOLUTIONS FOR THE TEST CASES

4.1 1D Dam Break Problem with Analytical Solutions

The developed code firstly tested for a generic 1D dam break problem for which analytical solutions are available. Analytical solutions give the time dependent water surface profile and depth averaged velocity for inviscid flow over a horizontal bed for a limited range of the physical domain. Initially hydrostatic water held behind a vertical wall is released by sudden removal of the vertical wall. Then all kind of surface waves can be observed depending on the initial water depths on upstream and downstream of the wall.

Numerical solutions for the same conditions are obtained and compared to the analytical solutions to verify capabilities of the mathematical model and the numerical solution technique adopted here. The analytical solution of the test case (Stoker, 1957), (Wu, Huang, & Zheng, 1999) , (Zoppou & Roberts, 2003) is defined in Table 4-1 . The channel is 2000 m long with an imaginary wall (dam) located at the midpoint of the channel (at x=1000 m). There are different stationary water levels at the left and right hand side of the wall and as initial condition the velocity is set to zero everywhere. By removal of the imaginary wall, a discontinuity is introduced to the flow at t=0 seconds. The aim in this test case is to observe the development of shock waves and rarefactions that will move to upstream and downstream at t=50 seconds. The results of this comparison have been shown in Figure 4-1 for supercritical case and Figure 4-2 for subcritical case. The computational results satisfactorily fit the analytical solutions. It is noteworthy that different limiters were tested and results were not affected significantly.

Table 4-1 Analytical solution for dam break problem in a wide frictionless open channel (Zoppou & Roberts, 2003)

Range	**Dependent Variable**
$x \le x_{gate} - t\sqrt{gh^L}$	$u = 0$ $h = h^L$
$x_{gate} - t\sqrt{gh^L} < x \le x_{gate} + t(u_2 - \sqrt{gh_2})$	$u = u_3 = \frac{2}{3}(\sqrt{gh^L} + \frac{x}{t})$ $h = h_3 = \frac{4}{9g}(\sqrt{gh^L} - \frac{x}{2t})^2$
$x_{gate} + t(u_2 - \sqrt{gh_2}) < x < x_{gate} + t\lambda^R$	$u = u_2 = \lambda^R - \frac{gh^R}{4\lambda^R}(1 + \sqrt{1 + \frac{8(\lambda^R)^2}{gh^R}})$ $h = h_2 = \frac{h^R}{2}\left(\sqrt{1 + 8(\frac{2h_2}{h_2 - h^R}\frac{\sqrt{h^L} - \sqrt{h_2}}{\sqrt{h^R}})^2} - 1\right)$
$x_{gate} + t\lambda^R \le x$	$u = 0$ $h = h^R$

Here the term λ^R, represents the shock speed and can be obtained by nonlinear equation below

$$\lambda^R = 2\sqrt{gh^L} + \frac{gh^R}{4\lambda^R}\left(1 + \sqrt{1 + \frac{8(\lambda^R)^2}{gh^R}}\right) - \left(2gh^R\sqrt{1 + \frac{8(\lambda^R)^2}{gh^R}} - 2gh^R\right)^{1/2} \qquad (4.1)$$

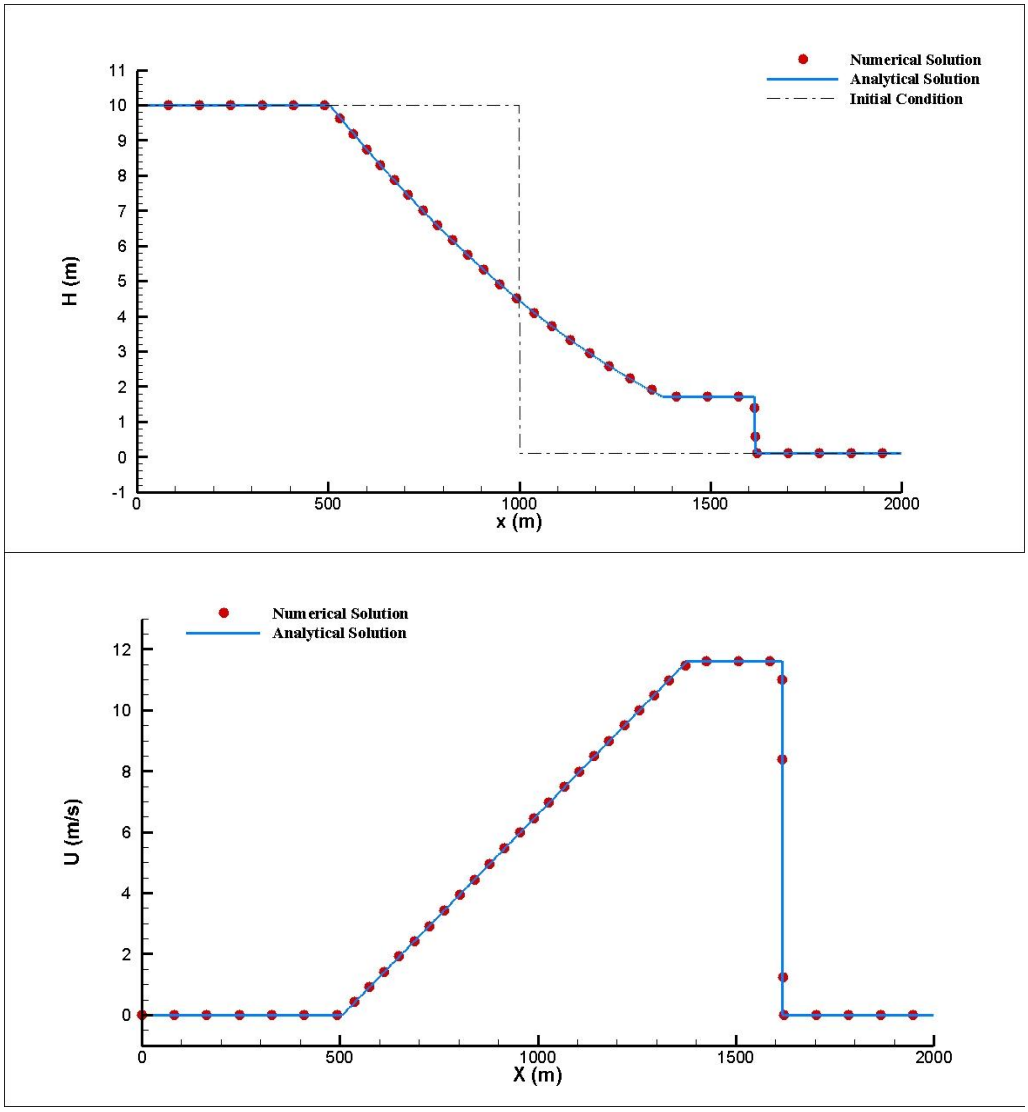

Figure 4-1 Comparison between numerical and analytical solution for 1D dam break test case at T=50sec, mesh size,Δx=2.00 m , H^L=10.00 m and H^R=0.10 m (supercritical flow), results obtained via HLL method.

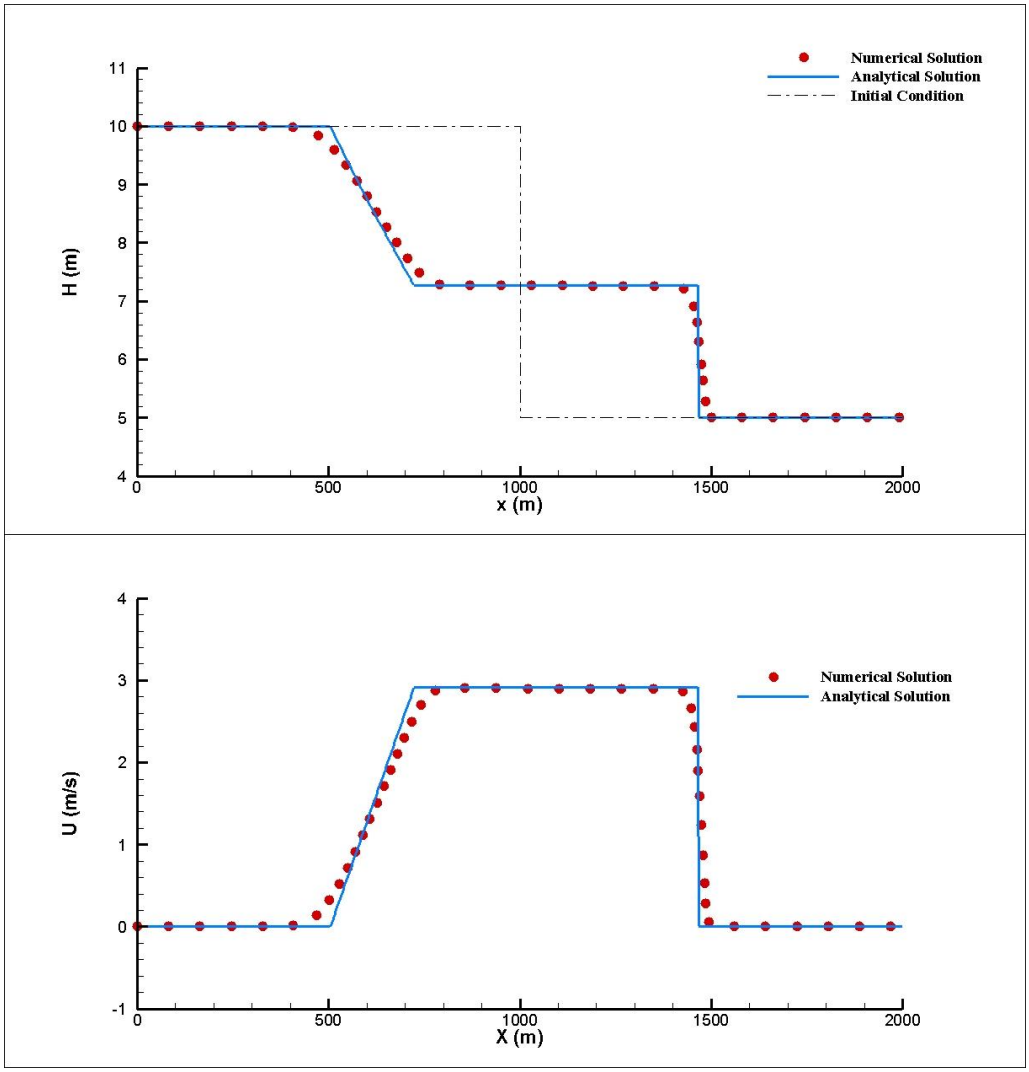

Figure 4-2 Comparison between numerical and analytical solution for 1D Dam Break test case at T=50sec, mesh size,Δx=2.00 m , H^L=10.00 m and H^R=5.00 m (subcritical flow), results obtained via HLL method.

4.2 1D Dam Break Problem in a Closed Domain with Various Bed Slopes

In the second test case the bottom slope is considered in addition to flow conditions of the first test case. However, there are no analytical solutions available for this case. A schematic description of the flow domain is shown in Fig.4.1. The initial condition in this test case is similar to classical dam break problem, the only difference is varying *h* values which are due to the sloped bed.

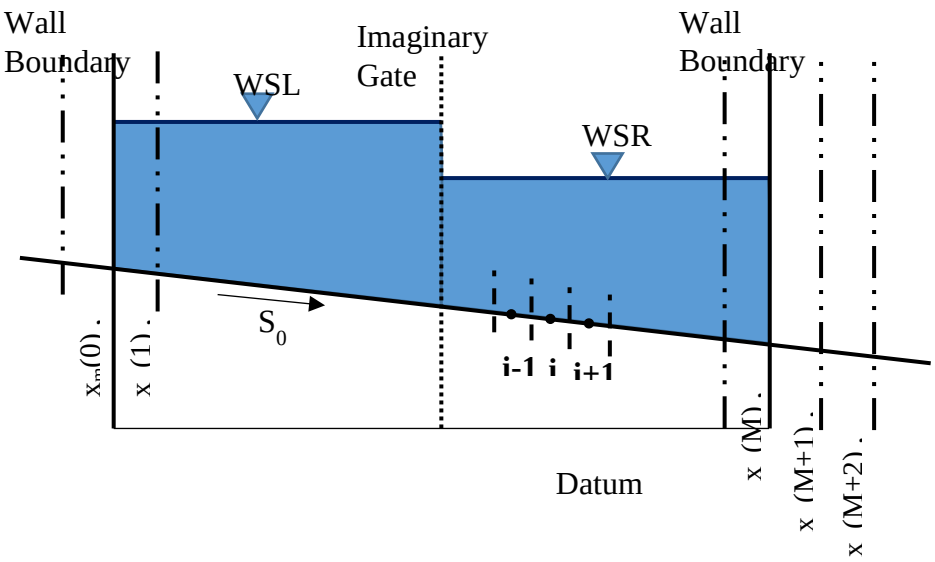

Figure 4-3 Dam break with various slope grid system

The main goal in this study is to observe the effects of some computational flow domain parameters on HLL method. One of the most important parameter that was focused on is the slope of the channel bed. In real life, considering a flood in an urban area, an obstacle like a building or a vertical wall can appear to cause a sudden change in bed slope and setting it to infinity. In order to focus on this problem, specific test cases have been defined and studied.

The numerical solution of 1D dam break problem does not require long processing times but animation of water surface deformation in a laptop computer may become troublesome when there are large number of data points in the domain. To facilitate video animations in a laptop computer the channel length is reduced to *1000* m and the wall is located at *500* m. Thus *50%* savings in computer memory and increased animation speeds were achieved.

4.2.1 Effect of Mesh Size in the Solution

One of the most important parameters in every simulation based on numerical methods is the size of the control volumes namely, mesh size. Thus, in order to see the role of mesh size on the solution, one of the cases has been studied for different

mesh sizes, Δx=1.0, 5.0 and 10.0 m. Water surface profiles at t=1000 s are shown in Figure 4-4, Figure 4-5 and Figure 4-6. For Δx=5. and 10. m cases surface profiles have some sharp variations which do not describe a water wave. When Δx=1.0 m such sharp variations disappear and a smooth water wave is observed. In rest of the study mesh sizes were chosen as 1 m or less.

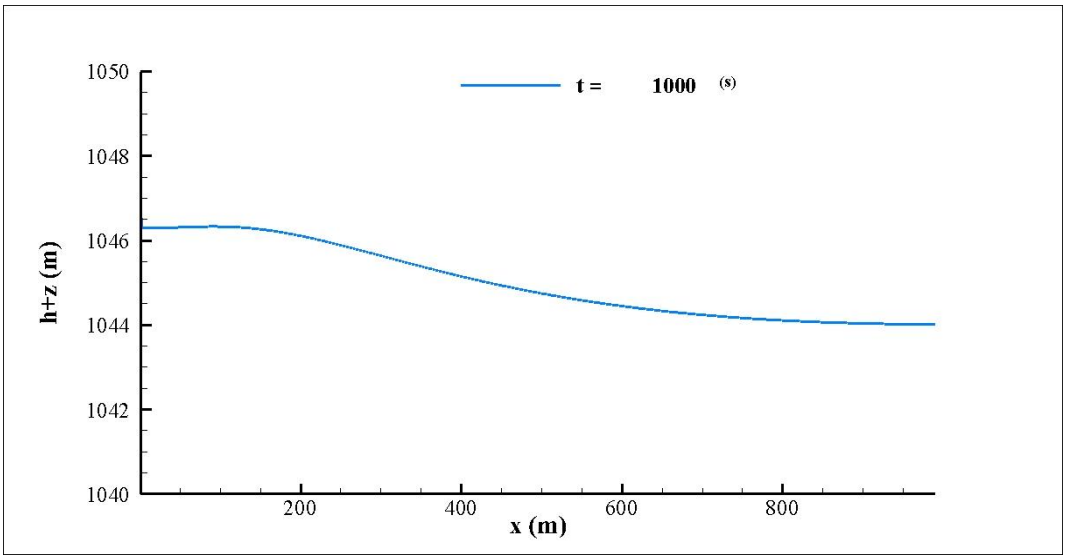

Figure 4-4 Mesh size comparison, S_0=0.4, Δx=1.0 m

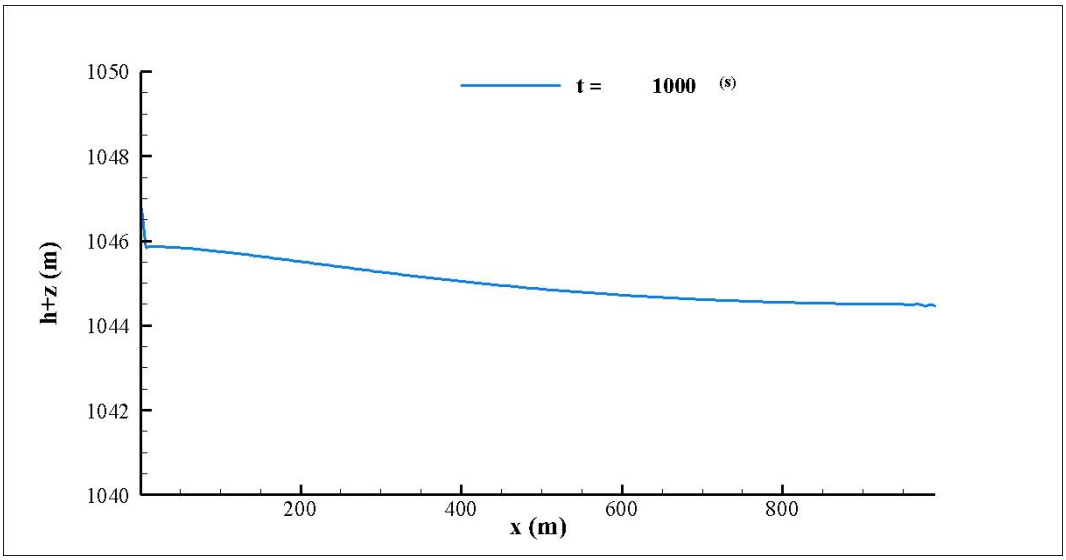

Figure 4-5 Mesh size comparison, S_0=0.4, Δx=5.0 m

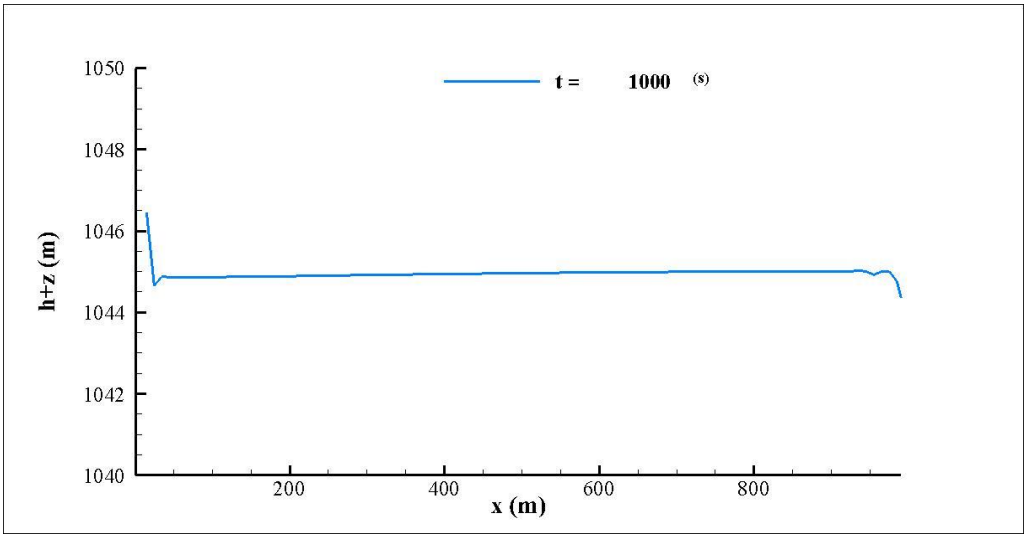

Figure 4-6 Mesh size comparison, S0=0.4, Δx=10.0 m

4.2.2 Effect of Bed Slope on the Solution

In this case different slopes from *0* to *1* have been studied for the same initial conditions. The total length of the domain is *1000* m, and the mesh size has been selected as 1m. An imaginary gate has been located at *x=500* m. A CFL number of *0.9* has been set in order to achieve the stability throughout the solution.

When the slope is large, a part of the channel can dry up at certain instances of the wave motion in the computational domain. Present algorithm cannot deal with negative water depths and therefore it is necessary to keep the whole computational domain all over the simulation time wet. Therefore, initial water depths in the computational domain are increased to provide positive water depth at all instants of simulation.

Solutions were repeated with different bed slopes starting from S_0=0. Computations were continued from the initial steady state to final steady state which is a horizontal water surface between the two end boundaries. The maximum bed slope on which the dam break problem can be solved is 1. For slopes more than this value, method develops unrealistic waves which cannot be treated by slope limiters. Some instantaneous water surface profiles of this simulation are shown in Figure 4-7 . In this case, $S_0=1.0$, it takes *5000* seconds to reach to final steady state.

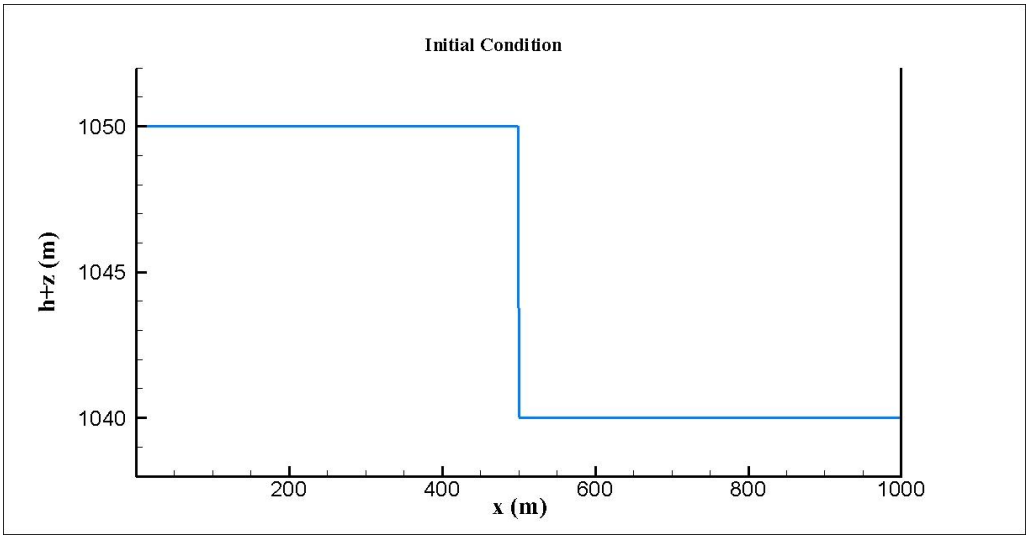

(a)

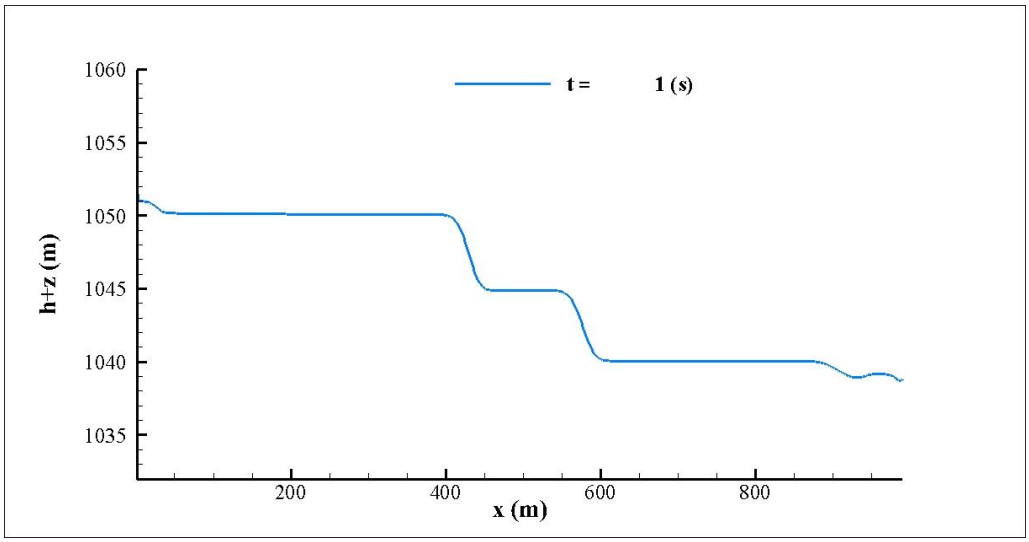

(b)

Figure 4-7 Instantaneous water surface profiles of test case simulation to investigate the effect of bed slope on the solution, S_0=1.0 , WSL=1050 (m), WSR=1040 (m), Δx=1.0 m, (a) T=0 s (initial condition), (b) T=1 s

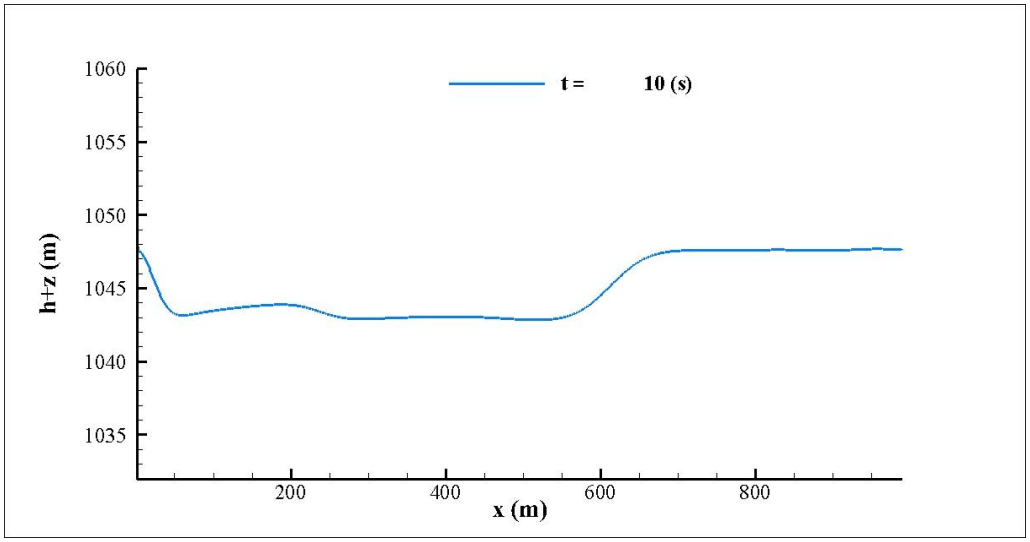

(c)

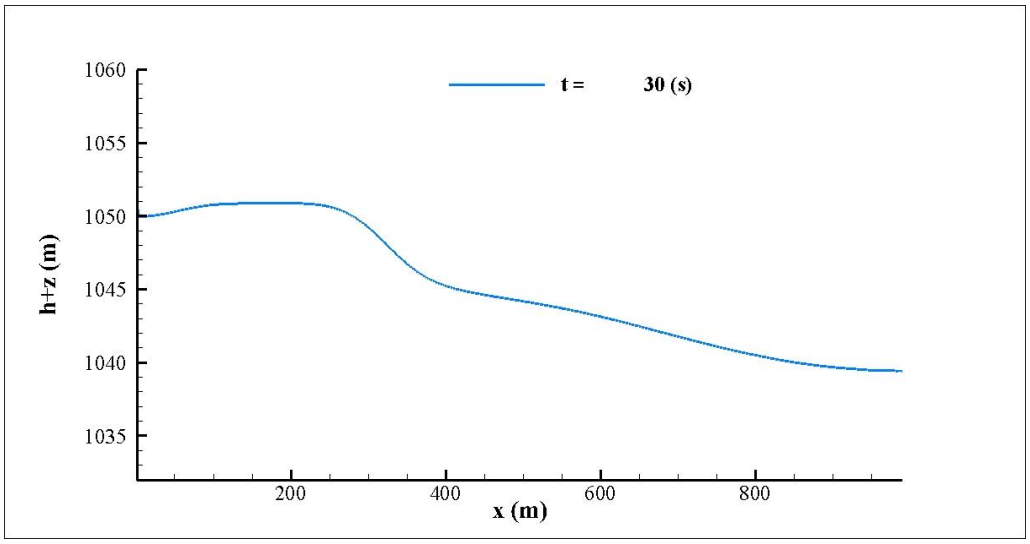

(d)

Figure 4-7(continued) Instantaneous water surface profiles of test case simulation to investigate the effect of bed slope on the solution, S_0=1.0, WSL=1050 (m), WSR=1040 (m), Δx=1.0 m, (c) T=10 s , (d) T=30 s

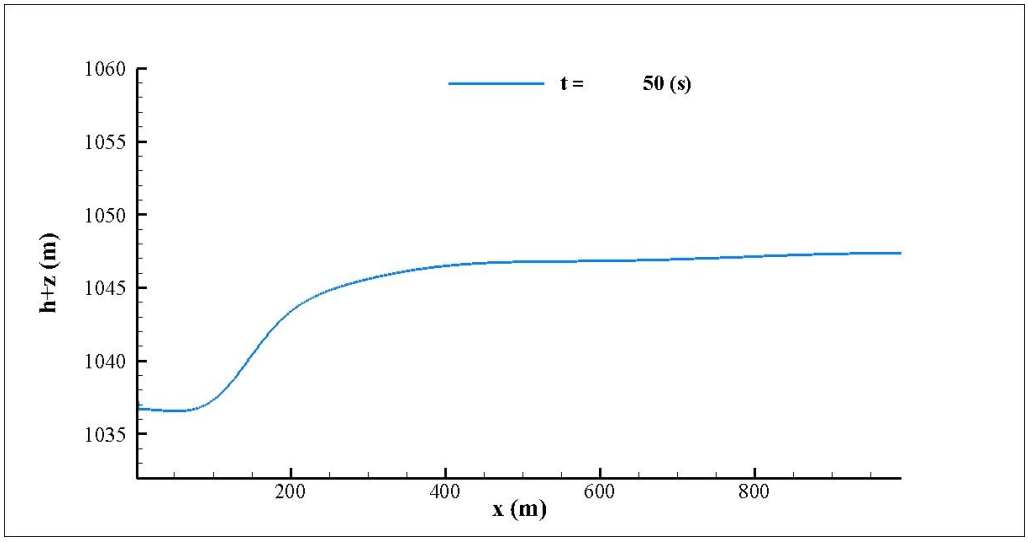

(e)

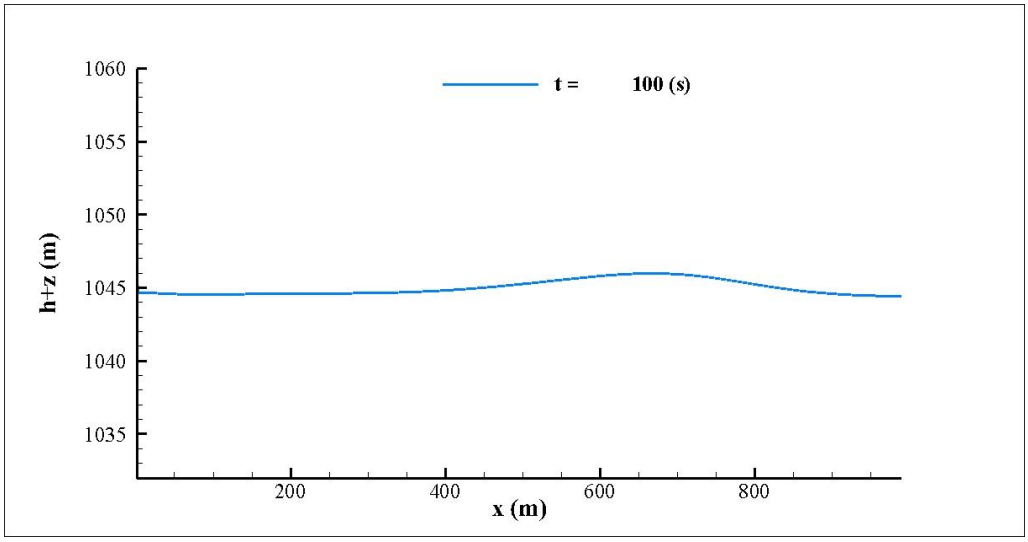

(f)

Figure 4-7(continued) Instantaneous water surface profiles of test case simulation to investigate the effect of bed slope on the solution, S_0=1.0, WSL=1050 (m), WSR=1040 (m), Δx=1.0 m, (e) T=50 s , (f) T=100 s

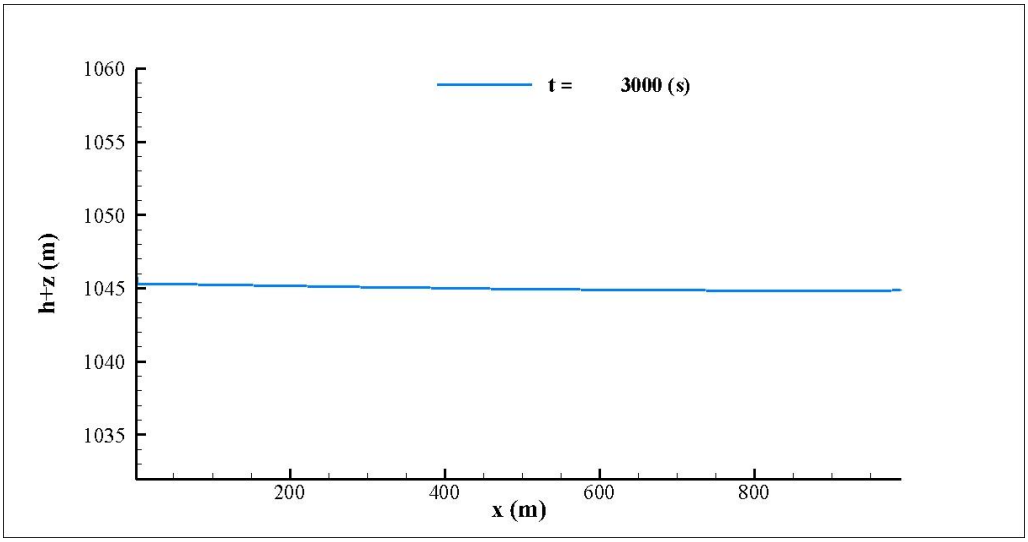

(g)

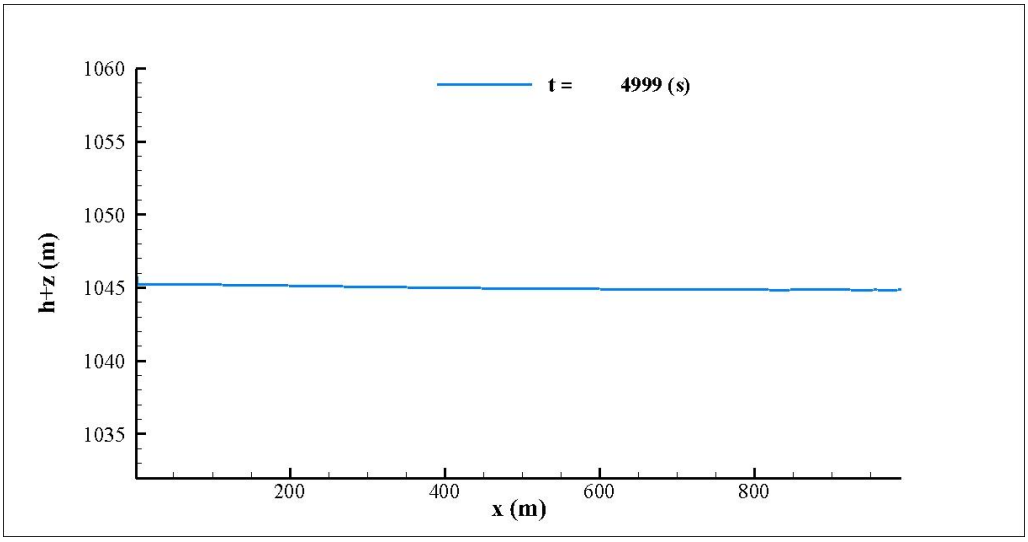

(h)

Figure 4-7(continued) Instantaneous water surface profiles of test case simulation to investigate the effect of bed slope on the solution, S_0=1.0, WSL=1050 (m), WSR=1040 (m), Δx=1.0 m, (g) T=3000 s , (h) T=4999 s

4.3 1D Dam Break Problem over a Step in a Closed Domain

In real life applications SWE may be solved in domains containing obstructions to flow. Flow around a completely submerged bed level discontinuity such as a prismatic step on the bed may disturb the flow and the numerical solution can sometimes be unrealistic. This test case of 1D dam break problem involves such a submerged step on the horizontal bed at the downstream of the imaginary dam (Figure 4-8). The wave motion over the step is investigated for various bed slope

evaluation algorithms. Depending on the grid resolution and location of the step, the bed slope may get different values at both ends of the step. For very fine mesh, at the upstream and downstream vertical faces of the step, the bed slope may be evaluated as very large (approaching infinity). Obviously, such a large value would dominate the other terms in the momentum equation and solution would fail. The bed slope in such cases should be calculated differently to alleviate the numerical problems due to large source term.

Modeling a vertical step in the numerical solution of SWE is physically not consistent with the assumptions made in the derivation of SWE. Therefore, one approach is to smooth the bed slope over the computational grid by a suitable technique. However, there should be certain criteria set to describe when and how much smoothing is necessary and appropriate.

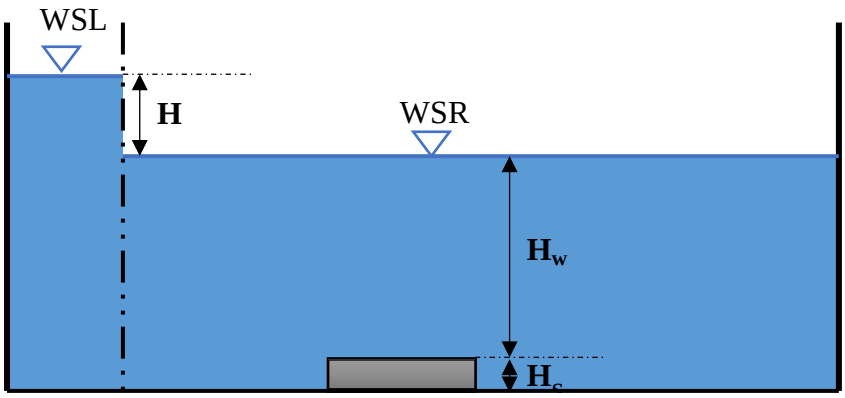

Figure 4-8 Dam break problem over a step on the bed

In calculating the bed slope, bed elevations at two neighboring grid points are used. Therefore, mesh size is a computational parameter that affects the slope computation (Figure 4-9). Bed slope (at the face of a step on the bed) is underestimated (smoothed) for large mesh sizes and this yields that the results would be more accurate as the mesh is refined. However, this can be a source of numerical instability or other computational problems such as spurious oscillations of the water depth.

Numerical tests are conducted to observe the water surface deformations as function of the bed slope computed at both ends of the totally submerged prismatic block on the bed. In this test case, mesh size was fixed as 0.5m. Then, block face angle was changed ($0<\alpha<90$) and water surface profiles were observed. It is observed for steep slopes of the block face there is an unphysical jump in water depth just above the two ends of it. To investigate the relationship between this spurious oscillations and other flow parameters, a series of tests have been conducted. The amplitude of these surface oscillation is defined by '*A*' (Figure 4-10). The ratio of *A* to the step height, H_s is plotted against face angle α in Figure 4-11. In all the cases the mesh size is 0.5 m and the total length of the domain is 500 m. Min-mod type limiter has been used and a total run time of 7000 seconds was considered. The imaginary gate is placed at x=100 m. The water level difference between two sides of the gates has been studied for two cases, 5 and 10 m. The other varying parameter is the height of the bottom step which has been studied for two cases of 5 and 10m. Test results parameters are summarized in Table 4-2 .

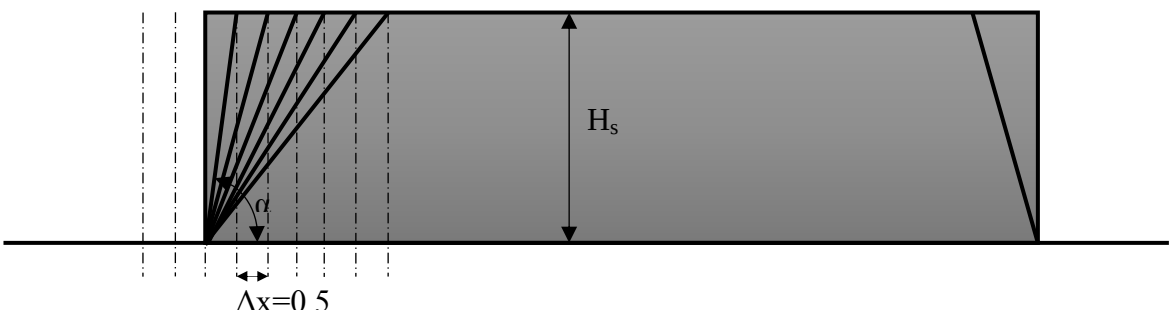

Figure 4-9 Bottom slope grid generation according to edge angle

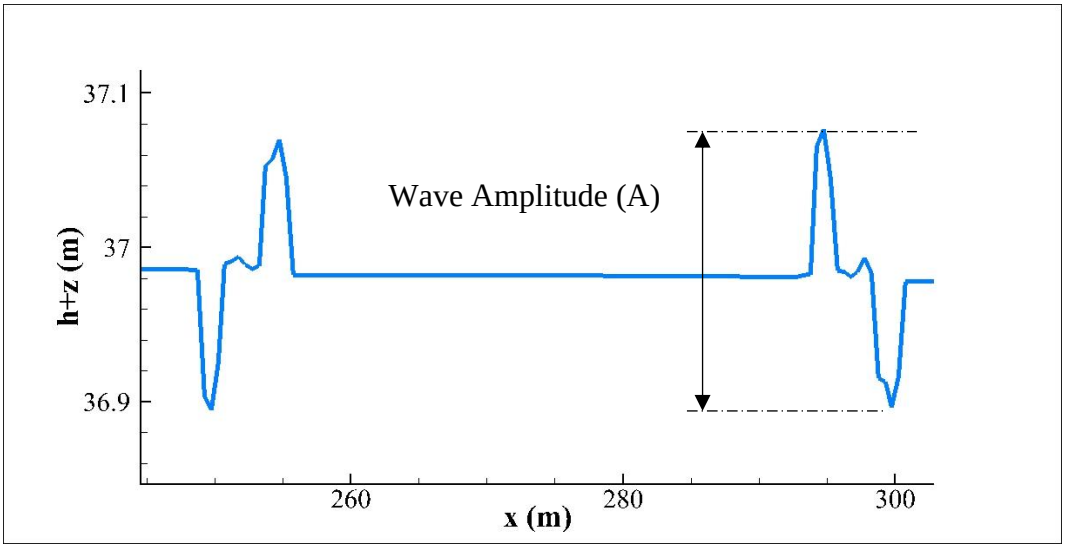

Figure 4-10 Wave formation around the geometry discontinuity at T=7000 sec

Table 4-2 General information of test case

Variable Name	**Value**
H_{step}	5 (m)
H_R	10 (m)
H_w	20 (m)
WSL	45 (m)
WSR	35 (m)
T	7000 (sec)
Δx	0.5 (m)
α	45^0
L_{domain}	500 (m)
L_{Step}	50 (m)

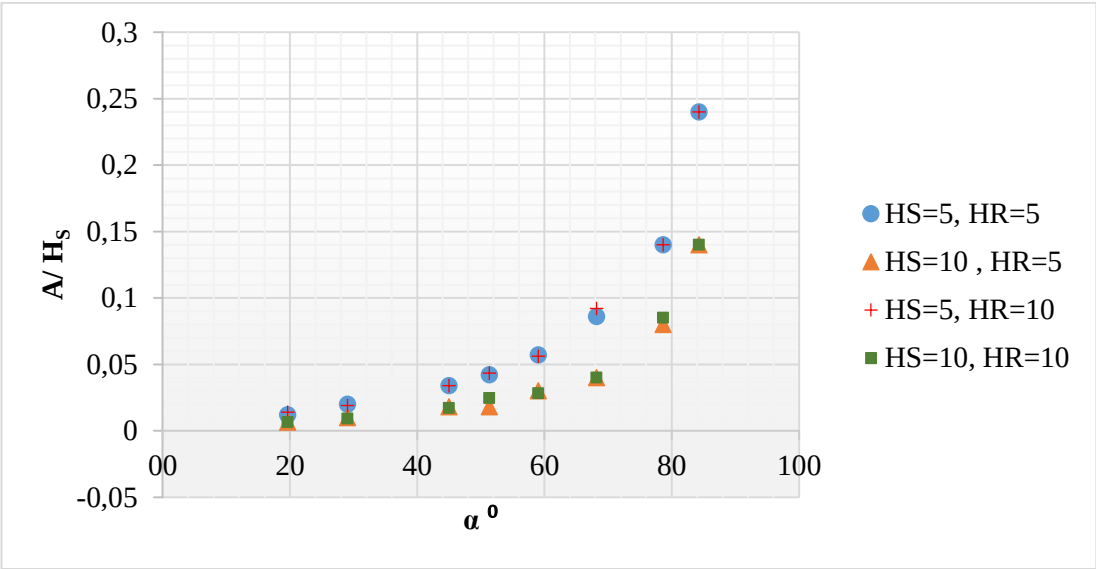

Figure 4-11 Relation between ratio of wave amplitude near discontinuity to step height and step edge angle

As seen in Figure 4-11 the unphysical surface oscillations are increasing with the face angle α as expected. Computations were repeated for different step heights, H_s, and for different water level difference, H_R. Results are independent of H_R but slightly dependent on H_s. In any case, α is the critical parameter. When α is less than 40^0 surface oscillations to step height ratio is less than 0.05 which is considered as negligible. However, for α>50^0 there is rapid growth of surface oscillations which may cause unrealistic spill of water to surroundings.

CHAPTER 5

CONCLUSIONS AND RECOMMENDATIONS

Shallow Water Equations are applied over channels with discontinuities in the bed elevation. HLL approximate Riemann solver is adopted to solve the SWE. Computer code was verified by comparing the numerical solutions to available analytical solutions. Two specific test cases involving 1D dam break problem has been studied.

The first case is a 1D dam break on a sloping bed with two wall boundaries at both ends. Water surface waves are observed from initial hydrostatic case to final hydrostatic case after development and diminishing of the dam break flow. Purpose of this test was to investigate appropriate boundary conditions while observing global volume conservation in the computational domain. It is found that simultaneous implication of 'no flow' boundary condition at both ends of the solution domain causes sources or sinks in the solution with continuous loss or increase of fluid volume. No relation with this erroneous behavior and the bed slope was found. The problem was solved by converting one of the boundary conditions to a constant water depth which is updated after each computational time step to conserve total fluid volume in the computational domain.

The second case is a dam break problem with totally submerged prismatic step located on the bed. When any water wave propagates over the step, a sharp wave-like non-physical deformation occurs above the corners of the step on the water surface. The surface deformations are caused by sudden changes in the bed slope due to front and back faces of the step. Depending on mesh size and location of step faces, the computed bed slope can be very large, approaching infinity for adequately fine mesh. Then large source term in the momentum equation becomes dominant and cause such non-physical oscillations. There is no cure for large slopes. The solution is to limit the bed slope to reasonable values to eliminate artificial water surface oscillations. It was shown that bed slopes above 1 should be avoided.

The existing slope limiters in the literature were put into test and despite the fact that no significant difference was spotted, some of the obtained results were detected as

being more dissipative in nature compared to the others. Based on the literature recommendations, the Min-Mod type slope limiter was chosen.

Present results were obtained with HLL approximate Riemann solver. It may be interesting to repeat present tests with some other Riemann solvers.

REFERENCES

Alcrudo, F., & Garcia-Navarro, P. (1993). A High Resoltion Godunov-type Scheme In Finite Volumes For the 2D Shallow Water Equations. *International Journal for Numerical Methods in Fluids, 16*, 489-505.

Alias, N., Liang, Q., & Kesserwani, G. (2011). A Godunov-type scheme for modelling 1D channel flow with varying width. *Computers & Fluids, 46*, 88-93.

Anastasiou, K., & Chan, C. (1997). Solutions of the 2D Shallow Water Equations Using Finite Volume Method on Unstructured Triangular Meshes. *International Journal for Numerical Methods in Fluids, 24*, 1225-1245.

Godlewski, E., & Raviart, P. (1996). *Numerical Approximation of Hyperbolic Systems of Conservation Laws.* New York: Springer.

Hussaini, M., Van Leer, B., & Van Rosendale, J. (1997). *Upwind and High Resolution Schemes.* Berlin: Springer-Verlag.

Murawski, K., Murawski, J., & Stpiczynski, P. (2012). Implementation of MUSCL-Hancock method into the C++ Code for the Euler Equations. *Bulletin of the Polish Academ of Science, 60*, 45-53.

Murillo, J., & Garcia-Navarro, P. (2012). Augmented versions of the HLL and HLLC Riemann solvers including source terms in one and two dimensions for shallow flow applications. *Journal of Computational Physics, 231*, 6861-6906.

Sorensen, R. M. (1993). *Basic Wave Mechanics for Coastal and Ocean Engineers.* New York: John Wiley & Sons Ltd.

Stoker, J. (1957). *Water Waves, The Mathematical Theory with Applications.* New York: Interscience Publishers, Inc.

Toro, E. F. (2001). *Shock Capturing Methods for Free Surface Shallow Flows.* Chichester: Wiley and Sonds Ltd.

Toro, E. F. (2009). *Riemann Solvers and Numerical Methods for Fluid Dynamics.* Berlin: Springer - Verlag Berlin Heidelberg.

Van Leer, B. (1977). Towards the Ultimate Conservative Difference Scheme III. Upstream–Centered Finite Difference Schemes for Ideal Compressible Flow. *Journal of Computational Physics, 23*, 263-275.

Van Leer, B. (2006). Upwind and High-Resolution Methods for Compressible Flow: From Donor Cell to Residual Distribution Schemes. *Communications in Computational Physics , 1*, 192-206.

Versteeg, H., & Malalasekera, W. (2007). *An Introduction to computational Fluid Dynamics* (Second ed.). London: Pearson Education Limited.

Wu, C., Huang, G., & Zheng, Y. (1999). Theoretical Solution of Dam-Break Shock Wave. *Journal of Hydraulic Engineering, 125*, 1210-1215.

Zia, A., & Banihashemi, M. (2008). Simple Efficient Algorithm (SEA) for Shallow Flows with Shock Waves on Dry and Irregular Beds. *International Journal for Numerical Methods in Fluids, 56*, 2021-2043.

Zoppou, C., & Roberts, S. (2003). Explicit Schemes for Dam-Break Simulations. *Journal of Hydraulic Engineering, 129*, 11-34.